

Silicate Weathering in the Semi-Arid Southern Pyrenees During the PETM: Lithium Isotope Evidence

Rocio Jaimes-Gutierrez¹, Marine Prieur¹, David J. Wilson², Philip A.E. Pogge von Strandmann^{2,3}, Emmanuelle Pucéat⁴, Thierry Adatte⁵, Jorge E. Spangenberg⁶, Sébastien Castellort¹

¹ Department of Earth Sciences, University of Geneva, Rue des Maraichers 13, 1205, Geneva, Switzerland
² London Geochemistry and Isotope Centre (LOGIC), Institute of Earth and Planetary Sciences, University College London and Birkbeck, University of London, Gower Street, London WC1E 6BT, UK
³ Institute of Geosciences, Johannes Gutenberg University Mainz, Mainz, Germany
⁴ Biogéosciences Dijon, Université Bourgogne Franche – Comté, UMR CNRS 6282, Dijon, France.
⁵ Institute of Earth Sciences, Géopolis, University of Lausanne, 1015 Lausanne, Switzerland
⁶ Institute of Earth Surface Dynamics, Géopolis, University of Lausanne, 1015 Lausanne, Switzerland

Correspondence to: Rocio Jaimes-Gutierrez, Rocio.JaimesGutierrez@univ.ch

Abstract

The Palaeocene-Eocene Thermal Maximum (PETM), a hyperthermal event ~56 Ma ago, allows the Earth system response to abrupt climate change to be explored. Recent investigations link the PETM with a negative lithium isotope ($\delta^7\text{Li}$) excursion, interpreted as an increase in continental silicate weathering fluxes, which can regulate Earth's surface temperature over geological timescales. However, the silicate weathering response under different climatic regimes has yet to be constrained. Here we aim to address the chemical weathering response to the PETM in the semi-arid Southern Pyrenees, and to explore how different archives (i.e. clays and carbonate nodules) record the weathering changes.

We investigated two continental sections in the southern Pyrenees. In the Esplugafreda section, we measured $\delta^7\text{Li}$ values as a silicate weathering proxy and ϵ_{Nd} values as a provenance proxy in the clay minerals. In the Rin section, we characterised the PETM locally by analysing $\delta^{13}\text{C}$ values in organic matter and examined the clay mineralogy in the paleosols, as well as measuring $\delta^7\text{Li}$ values in clays and carbonate nodules to trace silicate weathering. In the Esplugafreda section, we observe temporally stable ϵ_{Nd} values, while the $\delta^7\text{Li}_{\text{clays}}$ record shows two small positive excursions, one during the Pre-Onset Excursion (~0.7‰) and a second during the body of the PETM (~0.8‰). In the Rin section, the PETM is characterised by a negative carbon isotope excursion of 2.8‰. The clays consist mostly of illite/smectite, illite, kaolinite, and chlorite consistent with a seasonal climate in the region, and we find a positive $\delta^7\text{Li}_{\text{clays}}$ excursion of ~0.8‰.

The combined $\delta^7\text{Li}_{\text{clays}}$ and ϵ_{Nd} records indicate increased clay formation and increased silicate weathering fluxes in the semi-arid Pyrenees, while the sediment provenance was stable. The $\delta^7\text{Li}$ values in the carbonate nodules indicate more variability, potentially due to clay contamination. Constrained by the bedrock type of dominantly reworked sediments and the seasonal precipitation regime, the initially low weathering fluxes, despite a comparatively high weathering intensity, evolved towards higher weathering fluxes with enhanced erosion during the PETM.

Short Summary

How do semi-arid landscapes respond to rapid global warming? During the PETM—an extreme warming event 56 Ma ago—global lithium isotope records suggest an increase in weathering fluxes, and efficient negative feedback. In the Southern Pyrenees, however, we find the opposite signal: clay $\delta^7\text{Li}$ values became ~1‰ heavier, indicating enhanced clay formation despite stable sediment provenance. These results suggest that regional hydroclimatic conditions can decouple terrestrial signals from global averages.

Formatted: English (UK)

Deleted: ge

Deleted: ,

Deleted: and

Deleted: Constrained by the bedrock type of dominantly reworked sediments and the seasonal precipitation regime, the initially low weathering rate, despite a comparatively high weathering intensity, evolved towards a higher weathering rate with enhanced erosion during the PETM.

Formatted: Font: Symbol

Formatted: Superscript

Deleted: or

Deleted: This study examines how weathering in the Southern Pyrenees responded to a significant global warming event that occurred 56 million years ago. We found that changes in rainfall and erosion significantly influenced how minerals break down, and that the weathering response evolved from the continental interior to the marine environment. These results highlight regional variations in Earth's surface response to climatic perturbations and the processes at play in response to global warming.

69 **1. Introduction**

70
71 Continental silicate weathering is a critical feedback mechanism that stabilises Earth's climate over geological
72 timescales by regulating atmospheric CO₂ through the long-term carbon cycle (Walker et al., 1981; Raymo and
73 Ruddiman, 1992; Maher and Von Blanckenburg, 2023). Through the breakdown of silicate minerals, the transport
74 of cations in river systems, and the precipitation and burial of carbonates in the ocean, silicate weathering
75 sequesters atmospheric CO₂, acting as a natural climate thermostat. Understanding how this process responds to
76 abrupt climate change is essential for evaluating its capacity to modulate carbon fluxes under a range of future
77 warming scenarios.

78
79 The Palaeocene-Eocene Thermal Maximum (PETM), a hyperthermal event ~56 Ma ago, was related to the rapid
80 release of greenhouse gases that triggered a 5–8 °C global temperature increase over a geologically brief interval
81 (Kennett and Stott, 1991; Dickens et al., 1995; Zachos et al., 2003, 2008; Westerhold et al., 2009; McNerney and
82 Wing, 2011). Global records from the PETM suggest increases in silicate weathering fluxes (e.g. Hessler et al.,
83 2017; Pogge von Strandmann et al., 2021; Jaimes-Gutierrez et al., 2025; Rush et al., 2025), while some local
84 records have been interpreted to show increased weathering intensity (e.g. Ramos et al., 2022; Chen et al., 2023),
85 underscoring the potential for weathering to buffer atmospheric CO₂ during extreme warming events. In the
86 context of modern anthropogenic warming, these insights are crucial for understanding the capacity of natural
87 systems to mitigate rising CO₂ levels (Zeebe et al., 2016; Carmichael et al., 2017 and references therein).

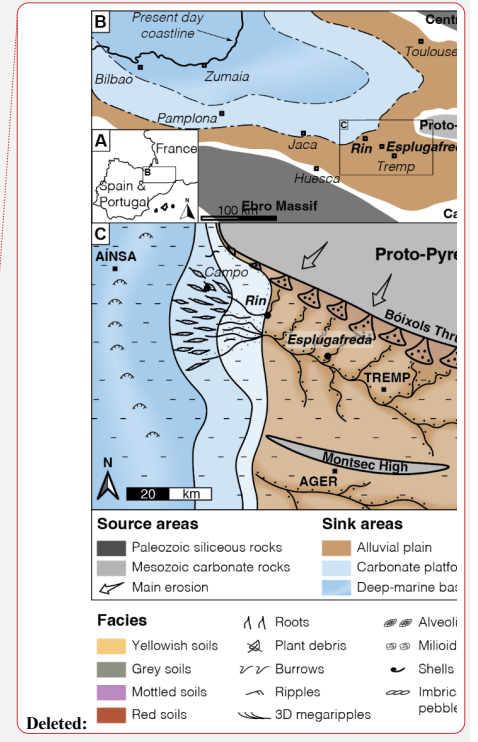
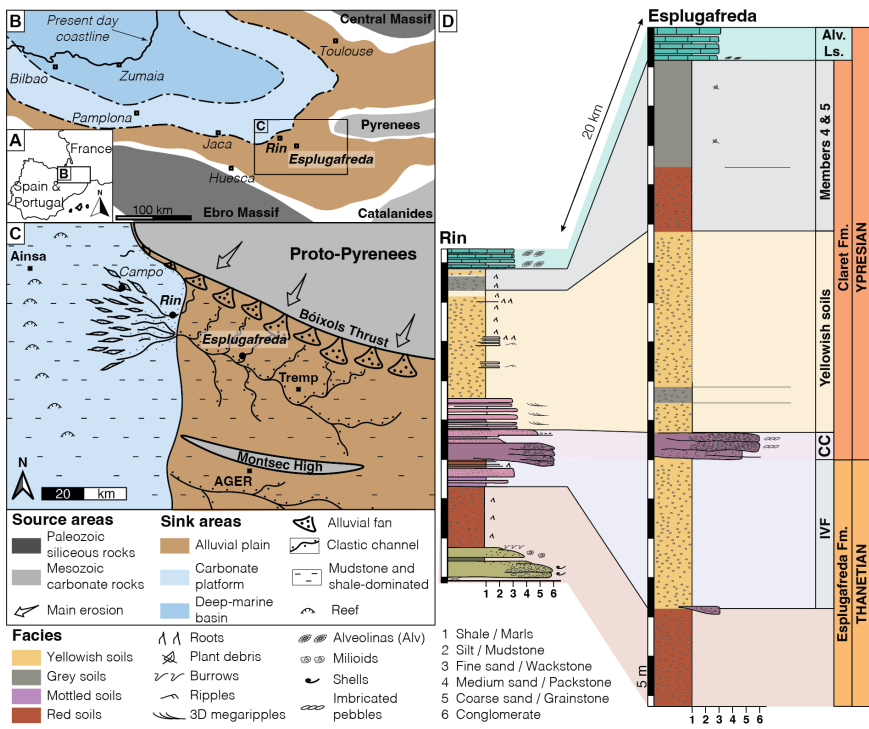
88
89 In mid-latitude records, a range of sedimentological, geochemical, and mineralogical proxies suggest that the
90 PETM resulted in a hydrological perturbation with episodic extreme rainfall events, increased seasonality, and
91 aridification, leading to a loss of vegetation, extreme flooding, and enhanced channel mobility (Schmitz et al.,
92 2001; Schmitz and Pujalte, 2007; Carmichael et al., 2017; Chen et al., 2018; Rush et al., 2021; Barefoot et al.,
93 2022; Vimpere et al., 2023). These changes were particularly pronounced in semi-arid regions such as the
94 Southern Pyrenees (~35°N paleolatitude, Fig. 1), where sedimentary records document hydrological seasonality,
95 enhanced erosion, and increased sediment transport (Schmitz and Pujalte, 2007; Pujalte et al., 2015; Chen et al.,
96 2018; Rush et al., 2021; Prieur et al., 2024, 2025; Jaimes-Gutierrez et al., 2024).

97
98 The Southern Pyrenees (Fig. 1) offer an exceptional setting for investigating climate-driven weathering dynamics.
99 This region experienced tectonic quiescence during the PETM (Rosenbaum et al., 2002), allowing for the isolation
100 of the effects of climate and hydrology on weathering. Sedimentary records indicate enhanced hydrological
101 seasonality and increased runoff, consistent with amplified denudation rates during this interval (Schmitz and
102 Pujalte, 2007; Pujalte et al., 2015; Rush et al., 2021). In this study, we use lithium isotopes ($\delta^7\text{Li}$) as a proxy for
103 silicate weathering and neodymium isotopes (ϵ_{Nd}) as a tracer for sediment provenance, in order to quantify the
104 weathering responses in the Southern Pyrenees and to assess their regional contribution to CO₂ regulation during
105 the PETM.

106
107 We focus on two continental floodplain sections to answer two primary questions: (i) What was the chemical
108 weathering response to the PETM in the semi-arid Southern Pyrenees? (ii) How do different sedimentary archives,
109 such as clays and carbonate nodules, record the weathering changes? In the Esplugafreda section, we measured
110 $\delta^7\text{Li}$ values in clay minerals as a weathering proxy, together with ϵ_{Nd} values in two clay size fractions to determine
111 sediment provenance. In the Rin section, we characterised the PETM locally through $\delta^{13}\text{C}$ measurements in
112 organic matter, and analysed the clay mineralogy of paleosols, and $\delta^7\text{Li}$ values in both clays and carbonate
113 nodules. These geochemical and mineralogical datasets allow us to reconstruct weathering dynamics in the region
114 and to assess how they compare with existing globally-distributed records of PETM weathering (Pogge von
115 Strandmann et al., 2021; Ramos et al., 2022; Chen et al., 2023; Jaimes-Gutierrez et al., 2025a; Rush et al., 2025).

- Formatted: English (US)
- Field Code Changed
- Formatted: English (US)
- Formatted: No underline
- Formatted: No underline
- Deleted: ,
- Deleted: its

- Deleted: lithium isotopes (
- Deleted:)
- Deleted: neodymium isotopes
- Deleted: (ϵ_{Nd})
- Formatted: French (Switzerland)



- Formatted: Not Highlight
- Formatted: French
- Formatted: French
- Formatted: French
- Field Code Changed
- Field Code Changed
- Formatted: French
- Formatted: French
- Field Code Changed
- Field Code Changed
- Formatted: Font: Italic
- Formatted: Font: Italic
- Formatted: Font: Italic
- Deleted: However, weathering efficiency peaks at intermediate erosion rates, while extremely thin or thick soils reduce weathering fluxes (Gabet and Mudd, 2009; Dixon and Von Blanckenburg, 2012; Bufer et al., 2024).
- Formatted
- Deleted: and increase with erosion

122
123
124
125
126
127

128

129
130
131
132
133
134
135
136

1.1. Silicate weathering as Earth's surface thermostat

Silicate weathering rates are influenced by climate (Dessert et al., 2003; West et al., 2005), vegetation (Moulton et al., 2000; Porder, 2019), lithology (Dessert et al., 2003; Caves et al., 2016; Murray and Jagoutz, 2024), and regolith properties (Kump and Arthur, 1997; Caves Rügenstein et al., 2019). Weathering is driven by the availability of fresh mineral surfaces, reactive fluids, and dissolution kinetics (Riebe et al., 2004; Bufer et al., 2021; Maher and Von Blanckenburg, 2023). Denudation ($D = \text{erosion rate } [E] + \text{silicate weathering } [W]$) links surface processes to the carbon cycle because erosion supplies fresh minerals, enhancing CO₂ sequestration through chemical weathering (Gaillardet et al., 1999; Riebe et al., 2004; West et al., 2005; Anderson et al., 2007; Hilton, 2023).

Two end-member regimes can be used to describe chemical weathering dynamics. In supply-limited regimes, mature soils dominated by secondary clays shield bedrock, limiting fresh mineral exposure and resulting in low weathering rates (Goddéris et al., 2008). In kinetically-limited regimes, which are typical of high-relief areas with thin soils, weathering rates are controlled by mineral dissolution kinetics (Kump et al., 2000; Riebe et al., 2004; West et al., 2005). Investigating how climate and erosion interact to shape these regimes under hyperthermal events such as the PETM is thus essential for understanding the weathering mechanisms and rates underpinning Earth's carbon cycle feedbacks in a warming climate.

150 **1.2. Lithium isotopes as a chemical weathering tracer**

151 Secondary clay minerals, which form as a by-product of primary silicate rock dissolution, preferentially
152 incorporate ⁶Li over ⁷Li, **resulting in isotopically light clays and isotopically heavy waters** (e.g., Pogge von
153 Strandmann et al., 2020). As weathering progresses, both **dissolved lithium** and the clays that precipitate from it
154 become isotopically heavier, with the $\delta^7\text{Li}$ value of the water and soil being linked by an approximately constant
155 fractionation factor (Pogge von Strandmann et al., 2021a). Measuring $\delta^7\text{Li}$ values in detrital and carbonate
156 archives therefore allows past weathering regimes to be reconstructed. Because carbonate weathering has a
157 minimal influence on riverine **lithium budgets**, **$\delta^7\text{Li}$ variations primarily reflect silicate weathering processes**
158 (Kisakürek et al., 2005). **Consequently**, lithium isotopes have become widely applied as a proxy for tracking clay
159 mineral formation, and thereby tracing silicate weathering intensity changes, both in modern systems (e.g.,
160 Dellinger et al., 2015, 2017; Pogge von Strandmann et al., 2023) and during past geological events (e.g., Misra
161 and Froelich, 2012; Pogge von Strandmann et al., 2013, 2021; Ramos et al., 2022; Jones et al., 2023).

163 Weathering congruency, which represents the balance between primary mineral dissolution and secondary clay
164 mineral formation, determines the $\delta^7\text{Li}$ composition of river waters and sediments (Dellinger et al., 2015; Zhang
165 et al., 2022 and references therein). **In rapidly eroding regions with low W/D , congruent weathering results in**
166 **minimal isotopic fractionation, because clay formation is relatively low (Fig. 2). In contrast, incongruent**
167 **weathering in soil-mantled environments with moderate W/D , such as floodplains with high clay formation, yields**
168 **both clays and waters with higher $\delta^7\text{Li}$ values (Fig. 2 and 3). Finally, in supply-limited regimes with high W/D ,**
169 **such as rainforests, there is no remaining primary rock material to weather, so pre-formed clays are re-dissolved,**
170 **which drives solutions to low $\delta^7\text{Li}$ values, but with a very low weathering flux (e.g., Dellinger et al., 2015). In**
171 **modern rivers, clays take up their Li from solution with an approximately constant fractionation factor (Pistiner**
172 **and Henderson, 2003; Pogge von Strandmann et al., 2023; Ramos et al., 2024), so their composition also mimics**
173 **this boomerang curve (Winnick et al., 2022; Pogge von Strandmann et al., 2023; Wei et al., 2025).**

175 In **detrital sediment archives**, only part of this boomerang trend is typically observed because of mixing of the
176 neoformed clays with primary silicate material, especially at low W/D conditions (Dellinger et al., 2017).
177 Therefore, continental and marine detrital records may need to be interpreted differently (e.g., Pogge von
178 Strandmann et al., 2021; Ramos et al., 2022, 2024; Jones et al., 2023; Jaimes-Gutierrez et al., 2025; Rush et al.,
179 2025; Wei et al., 2025). Because **finer sediment fractions tend to be preferentially transported further offshore due**
180 **to hydrodynamic sorting during river to marine transport, clay-sized records may be more clearly expressed in**
181 **some marine sedimentary records (e.g., Gibbs, 1977; Liu et al., 2023). Such biases resulting from mixing with**
182 **primary silicate grains in bulk sediment samples can potentially be reduced by analysing the clay size fraction (<2**
183 **μm), although this fraction can still also contain some primary minerals.**

185 Finally, **lithium isotopes can also be fractionated by direct climatic fluctuations. For example, temperature (Vigier**
186 **et al., 2008; Li and West, 2014) and hydrological controls (Zhang et al., 2022) have both been found to influence**
187 **the $\delta^7\text{Li}$ composition of river water, and consequently the composition of the sedimentary archives that form in**
188 **equilibrium with them (Pogge von Strandmann et al., 2023). In particular, riverine dissolved $\delta^7\text{Li}$ values have**
189 **been shown to have a negative correlation with runoff, because it controls the water-rock residence time that**
190 **affects clay formation, with the dry season exhibiting enhanced clay formation and higher $\delta^7\text{Li}$ values than the**
191 **wet season (Wilson et al., 2021; Zhang et al., 2022).**

193 **A detailed discussion on the lithium isotope interpretative framework, including the roles of grain size,**
194 **hydrodynamic sorting, and lithology, is provided in Jaimes-Gutierrez et al. (2025, Supplemental Material).**

195

Deleted: which leads to clays that are

Deleted: that are isotopically heavy ... ADDIN ZOTERO_ITEM CSL_CITATION {"citationID":"a14lu3lsm1g","properties":{"formattedCitation":"\u2014 (Pogge von Strandmann et al., 2020)"},"plainCitation":"(Pogge von Strandmann et al., 2020)","dontUpdate":true,"noteIndex":0},"citationItems":[{"id":"1037","uris":["http://zotero.org/users/6525398/items/RDBB BJMT"],"itemData":{"id":"1037","type":"article-journal"},"abstract":"Lithium and its isotopes can provide information on continental silicate weathering, which is the primary natural drawdown process of atmospheric CO2 and a major control on climate. Lithium isotopes themselves ... [2]

Formatted ... [1]

Deleted: Li

Formatted: English (UK)

Deleted: (clay)

Deleted: Li

Deleted: concentrations

Deleted: even in carbonate-dominated terrains, ...⁷Li v ... [3]

Formatted: English (UK)

Formatted: English (UK)

Deleted: Hence

Formatted: English (UK)

Deleted: ... Dellinger et al., 2015, 2017; Pogge von ... [4]

Deleted: In modern rivers, lithium isotopes in both the ... [5]

Formatted: Font: Italic

Deleted: 3

Formatted ... [6]

Deleted: to low

Deleted: ... Dellinger et al., 2015). In modern rivers, c ... [7]

Deleted: y

Deleted: are ... Iso expected to ... imics this boomerang ... [8]

Deleted: However, we note that under high W/D condit ... [9]

Formatted: English (UK)

Deleted: bulk

Deleted: river sediment samples

Formatted: English (UK)

Formatted ... [10]

Deleted: (Gibbs, 1977; Liu et al., 2023)

Formatted ... [11]

Deleted: fewer of the coarser-grained primary mineral ... [12]

Deleted: s...ch biases resulting from mixing with prim ... [13]

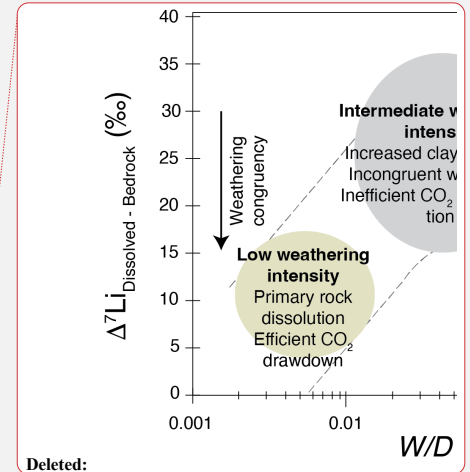
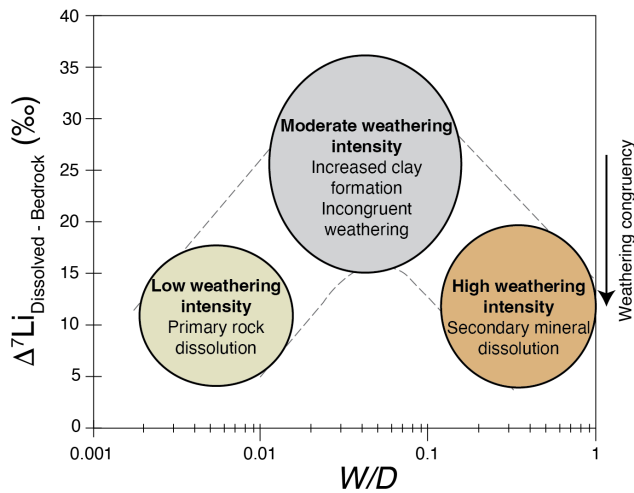
Formatted: English (UK)

Deleted: we note that l

Formatted: English (UK)

Formatted: English (UK)

Formatted ... [14]



Deleted:

346

347

348

349

Figure 2. Large-river dissolved lithium isotope composition ($\delta^7\text{Li}_{\text{dissolved}}$) corrected for bedrock composition ($\Delta^7\text{Li}_{\text{dissolved-bedrock}}$) plotted versus weathering intensity (W/D). Modified from Dellinger et al. (2015) and references therein.

350

351

352

353

354

355

356

357

358

359

360

361

362

363

364

365

366

367

During the PETM, Pogge von Strandmann et al. (2021) documented a ~3‰ negative $\delta^7\text{Li}$ excursion in several marine carbonate sections, indicating globally enhanced weathering fluxes (50–60%) and erosion rates (2–3x), and a shift to an overall lower weathering intensity regime. At a continental scale, detrital lithium isotope records from North America show coherent negative $\delta^7\text{Li}$ excursions in both floodplain and deep-marine settings, indicating rapid propagation of erosion- and weathering-related signals through sediment-routing systems under intensified hydrological conditions, despite largely stable sediment provenance, (Ramos et al., 2022; Jaimes-Gutierrez et al., 2025a; Rush et al., 2025). On a regional scale, Ramos et al. (2022) reported a rapid, sustained increase in silicate weathering intensity in the Bighorn Basin floodplains that was attributed to seasonal hydrological variability. Similarly, Chen et al. (2023) identified a ~100% increase in silicate weathering intensity in the Nanyang Basin, East Asia. These studies highlight the roles of local hydrology, lithology, and erosion in shaping regional weathering responses and the associated $\delta^7\text{Li}$ changes. However, they also reveal significant gaps in our understanding of how regional processes integrate into driving global $\delta^7\text{Li}$ records and carbon cycle feedbacks. Notably, discrepancies between the proposed increases in weathering intensity at a regional scale (Ramos et al., 2022; Chen et al., 2023) and the inferred decrease at a global scale (Pogge von Strandmann et al., 2021; Jaimes-Gutierrez et al., 2025a; Rush et al., 2025) require further assessment of how regional climatic and geological controls translate into weathering responses.

Deleted: ¶

Formatted: Normal

Formatted: Font: 10 pt

Formatted: Font: Symbol, 10 pt

Formatted: Font: 10 pt, Superscript

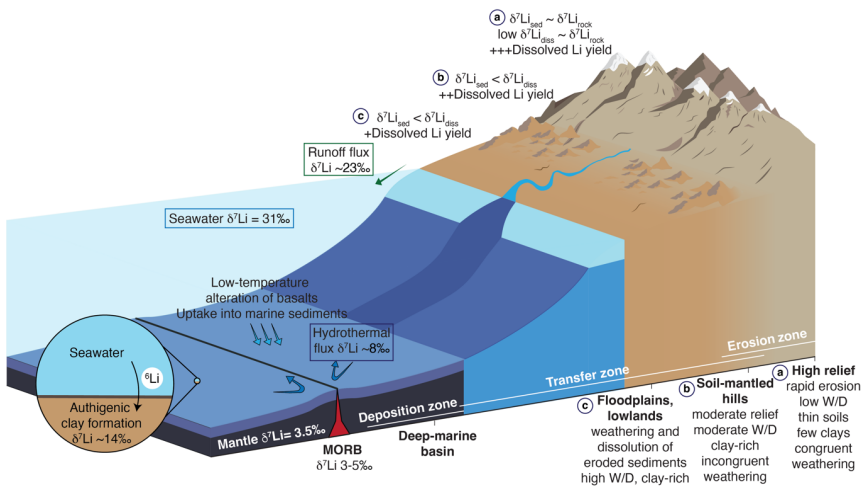
Formatted: Font: 10 pt

Formatted: English (UK)

Formatted: French (Switzerland)

Formatted: English (US)

Formatted: Font colour: Auto



370
371 **Figure 3.** Processes determining the lithium isotope composition of bulk sediments ($\delta^{17}\text{Li}_{\text{sed}}$) and dissolved lithium
372 flux along a sediment routing system from source to sink in relation to denudation. The weathering intensity (W/D)
373 expresses the relative share of weathering (W) over denudation (D), where $D = W + E$ (erosion). Modified from
374 Tofelde et al. (2021), Pogge von Strandmann et al. (2021a), and Bufe et al. (2024).

375
376 To address these gaps, we focused on the silicate weathering response to the PETM climatic perturbation in two
377 sections of the Southern Pyrenees (Espugafreda and Rin, Fig. 1). With its semi-arid climate, seasonal precipitation,
378 and relatively unreactive lithologies comprising reworked sediments and significant carbonate content (e.g.
379 Eichenseer, 1988; Eichenseer and Luterbacher, 1992; Gómez-Gras et al., 2016), this setting represents a
380 contrasting regional weathering regime to previous PETM studies. Our results contribute to understanding how
381 floodplain paleosols, which are often overlooked in global weathering studies, respond to climatic perturbations,
382 with broader implications for the recovery of Earth's climate system after significant warming events.

383 2. Geological context

384 The Pyrenees formed as a result of convergence between the Iberian and European plates, a process that initiated
385 in the Late Cretaceous and continued into the Miocene (Mattaier and Henry, 1974; Roure et al., 1989; Roest and
386 Srivastava, 1991; Rosenbaum et al., 2002). The orogenic evolution began with the mid-Cretaceous hyper-
387 extension of the Iberian margins, followed by the late Cretaceous subduction and collision with the European
388 plate (Teixell et al., 2016). Foreland basins formed on both sides of the fold and thrust belt (Puigdefbregas and
389 Souquet, 1986; Muñoz, 1992; Gómez-Gras et al., 2016). The Southern Pyrenean foreland basin was active
390 between the Late Cretaceous and the Oligocene, and contains well-preserved sedimentary archives of continental
391 and marine environments.

392
393 The Tremp-Graus Basin is located in the South-Central Pyrenean Foreland Basin (Spain), delimited by the Boixols
394 Thrust to the north and the Montsec Thrust to the south (Fig. 1C). During the Palaeocene, the Tremp-Graus Basin
395 was dominated by continental sedimentation sourced from the Pyrenees (Gómez-Gras et al., 2016). The
396 continental deposits of the Thanetian Espugafreda Formation (Fm.) predominantly represent floodplain sediment
397 accumulation and consist of clay, silt, carbonate nodules, and Microcodium grains, with some isolated sandy to
398 conglomeratic channels (Puigdefbregas and Souquet, 1986; Dreyer, 1993; Schmitz and Pujalte, 2003, 2007).

399 2.1. Espugafreda section

400 The Espugafreda section (42°14'50" N; 0°45'13" E, Fig. 1B) has been widely studied for its well-preserved
401 Palaeocene-Eocene sedimentary record (Schmitz and Pujalte, 2003; Baceta et al., 2005; Khozyem, 2013; Tremblin
402 et al., 2022; Basilici et al., 2022; Jaimes-Gutierrez et al., 2024) (Fig. 1D). The Upper Thanetian sediments belong
403 to the Espugafreda Fm. in the Tremp Group of the Tremp-Graus Basin (Dreyer, 1993). This formation consists
404 of coarse-grained stream deposits intercalated with red floodplain sediments that are rich in carbonate nodules

Deleted: ,

Deleted: resulted

Deleted: in

Formatted: English (UK)

Deleted: The

409 and characterised by mature paleosols. The PETM sediments have been classified into five stratigraphic members
 410 (Pujalte and Schmitz, 2005; Pujalte et al., 2014; Colomera et al., 2017; Basilici et al., 2022). Member 1 belongs
 411 to the Esplugafreda Fm. and consists of a fining-upwards sequence of conglomerates and cross-laminated
 412 sandstones, known as the Incised Valley Fill (IVF) sediments. During this interval, a first negative carbon isotope
 413 excursion (CIE) marks the Pre-Onset Excursion (POE) (Khozyem, 2013; Tremblin et al., 2022). Member 2 at the
 414 onset of the Ypresian is represented by the Claret Conglomerate (Pujalte and Schmitz, 2005), a 3-5 m thick
 415 conglomeratic unit, corresponding to a braid plain which has been interpreted as the proximal part of a megafan
 416 (Schmitz and Pujalte, 2007). Member 3, the Yellowish soils, consists of yellow mudstone with purple mottling,
 417 and the main body of the CIE is recorded during this interval (Pujalte and Schmitz, 2005). Member 4, consisting
 418 of red soil with gypsum, and Member 5, comprising light red mudstones with scarce carbonate nodules,
 419 correspond to the recovery interval of the PETM in this locality (Pujalte and Schmitz, 2005; Baceta et al., 2011;
 420 Khozyem, 2013; Pujalte et al., 2014; Tremblin et al., 2022; Basilici et al., 2022).

421 **2.2. Rin section**

422 The Rin section (42°19'42.01"N; 0°32'42.16"E, Fig. 1B and Fig. 4) is a Palaeocene-Eocene sequence comprising
 423 mudstone-dominated alluvial deposits and very shallow marine carbonate alternations, indicating episodes of
 424 transgression and regression on the coastal plain (Schmitz and Pujalte, 2007) (Fig. 1). The upper Esplugafreda
 425 Fm. soils are characterised by grey mottling and sparse iron nodules, with preserved pedogenic features such as
 426 peds. Member 1, the IVF, consists of 4 m-thick reddish-yellow soils that are rich in carbonate nodules. Member
 427 2, the Claret Conglomerate, outcrops as a 3 m-thick calcareous conglomerate with pale red clay pockets, and has
 428 sparse carbonate nodules and charophyte occurrences. Member 3, the Yellowish soils, consists of 13 m-thick
 429 reddish-yellow clays and silts. The base of Member 3 records sparse occurrences of lignite and carbonate nodules.
 430 Member 4 is not preserved in the Rin section, and the upper 3 m of the sequence consists of Member 5, which has
 431 light grey to reddish yellow soils with grey mottling, before the overlying Alveolina Limestone.
 432

Deleted: osed of

Deleted: The

Deleted: a

Deleted: c



433 **Figure 4.** Rin section between the upper Thanetian and lower Ypresian. Members 1-5 described in the literature
 434 for the Esplugafreda section can be identified in the Rin section, except that Member 4 from the recovery phase
 435 of the PETM has not been preserved. E. Fm.: Esplugafreda Formation.

437 **3. Material and methods**

438 **3.1. Size fraction separation**

439 Standard protocols (e.g. Adatte et al., 1996; Bauer et al., 2016) were followed for decarbonation and size fraction
 440 separation at the Institute of Earth Sciences clay laboratory at the University of Lausanne (ISTE-UNIL). Samples
 441 (~5 g) were leached with 10% HCl for 30 min in a bubble bath, including 3 min in an ultrasonic bath, to
 442 disaggregate sediments and dissolve calcite. Distilled water was used to remove the acid until a neutral pH was
 443 obtained. Subsequently, the <2 µm fraction was separated by settling and enhanced with a centrifuge. Settling and
 444 extraction were repeated three times.

Deleted: ,

445 **3.2. Clay mineralogy**

446 The clay minerals were identified on air-dried and ethylene glycol-solvated samples at ISTE-UNIL following the
 447 protocol described in Adatte et al. (1996). An aliquot of the separated size fractions was pipetted on glass slides
 448 and dried at room temperature. The air-dried samples were further analysed with a Thermo Scientific ARL X'TRA
 449 powder diffractometer equipped with a Cu anode, operated at 45 kV and 40 mA. The step size was 0.02, with a
 450 scan rate of 0.5-1.2/min. Samples were glycolated to identify smectite (Moore and Reynolds, 1992).

456 Diffractograms were analysed using the XRDWin software, where the background was removed, and a
457 deconvolution was performed for overlapping peaks (e.g. K002 and Ch004).

Deleted: ,

458 3.3. Nodule purification

Deleted: P

459 Carbonate nodules were washed with running distilled water until visible clay clumps were removed. They were
460 then placed in a beaker with distilled water and in an ultrasonic bath to remove the remaining clay particles. A
461 second round in the ultrasonic bath was then carried out with some drops of 10 M HCl in order to remove the
462 outermost layer. The nodules were later washed in running distilled water, dried at 40 °C, and ground.

Deleted: 10 M

Deleted: e

463 3.4. Rock-Eval pyrolysis

Deleted: P

464 Organic matter analyses were performed on powdered bulk rock samples using a Rock-Eval 6 at ISTE-UNIL,
465 following standard methodology (Espitalie et al., 1985; Behar et al., 2001). For calibration, the IFP 160000
466 standard was used. The Rock-Eval pyrolysis parameters measured were hydrogen index (HI, mg HC/g TOC, HC
467 = hydrocarbons), oxygen index (OI, mg CO₂/g TOC), Tmax (°C), and total organic carbon content (TOC, wt.%).
468 The HI, OI, and Tmax values give an overall measurement of the type and degree of maturation of the organic
469 matter (e.g. Espitalie et al., 1985).

Deleted: ,

470 3.5. Isotope geochemistry

471 3.5.1. Organic matter carbon isotopes

472 The carbon isotope composition of the decarbonated bulk rock samples was determined at the Institute of Earth
473 Surface Dynamics at the University of Lausanne (IDYST-UNIL) by elemental analysis/isotope ratio mass
474 spectrometry (EA/IRMS). The EA/IRMS system consisted of a Carlo Erba 1108 (Fisons Instruments, Milan, Italy)
475 elemental analyser connected to a Delta V Plus isotope ratio mass spectrometer via a ConFlo III split interface
476 (both Thermo Fisher Scientific, Bremen, Germany) operated under continuous helium (He) flow (Spangenberg,
477 2006; Spangenberg and Zufferey, 2019). The carbon isotope compositions were reported in the delta (δ) notation
478 as permil (‰) variations of the molar ratio of the heavy to light isotope (¹³C/¹²C) relative to the international
479 standard Vienna Pee Dee Belemnite limestone (VPDB). For calibration and normalisation of the measured δ¹³C
480 values to the Vienna Pee Dee Belemnite limestone (VPDB) standard, a four-point calibration was used with
481 international reference materials and in-house standards (Spangenberg and Zufferey, 2019). The used standards
482 included UNIL-Glycine (δ¹³C = -26.10 ± 0.05‰), UNIL-Urea-1 (δ¹³C = -43.00 ± 0.04‰), UNIL-Pyridine (δ¹³C
483 = -29.25 ± 0.06‰), and the RM USGS24 graphite (δ¹³C = -16.05 ± 0.04‰). Analyses were done in duplicates.
484 The accuracy of the analyses was checked periodically through the analysis of international RM standards not
485 used for calibration. The reproducibility and precision of the EA/IRMS δ¹³C analyses were determined by the
486 standard deviation of separately replicated analyses and were better than 0.1‰.

Formatted: Adjust space between Latin and Asian text,
Adjust space between Asian text and numbers

Formatted: Font: 10 pt

Deleted: For calibration and normalisation of the measured
δ¹³C values to the international scales (VPDB-LSPVEC
lithium carbonate scale), a 4-point calibration was used with
international reference material (RM) and in-house standards

Formatted: English (US)

Formatted: Font: 12 pt, Font colour: Auto

487 3.5.2. Lithium isotopes

488 Sample digestion, column chemistry, and mass spectrometry were conducted in the London Geochemistry and
489 Isotope Centre (LOGIC) laboratories at University College London (UCL) and Birkbeck, University of London.
490 Clay samples were subjected to bulk digestion using concentrated HF, HNO₃, and HClO₄ in Teflon beakers on a
491 hot plate at 130 °C, followed by steps in concentrated HNO₃ and 6 M HCl. The carbonate nodules were subject
492 to leaching to separate the carbonate and detrital fractions. The carbonate fraction was extracted by leaching ~100
493 mg of sample in 8 ml 0.1 M HCl for 1 h (Pogge von Strandmann et al., 2013; Wilson et al., 2021), allowing a
494 maximum of ~40 mg of calcium carbonate to be dissolved.

495 A standard method of elution was applied for lithium isotope separation in 0.2 M HCl. Two-column passes were
496 applied through AG50W-X12 resin to ensure matrix removal (Pogge von Strandmann et al., 2013). Given that
497 lithium isotopes are fractionated during ion chromatography, sample splits were collected before and after the
498 lithium collection interval to assess column yields. For example, a 1% loss in yield at UCL has been assessed to
499 lead to an offset of 1.7‰ (Wilson et al., 2021). Here, yields between two column passes were 99.8-100%,
500 indicating excellent recovery.

501 Lithium isotope measurements were performed on a Nu Plasma 3 MC-ICP-MS at UCL, using a Cetac Aridus 2
502 desolvation system, 'super-lithium' cones, and standard-sample bracketing with the IRMM-016 Li standard
503 (Pogge von Strandmann et al., 2019). Samples were measured at least three times within an analytical session,
504 with each measurement integrating ~50 s, and the reported values are the mean and standard deviation (2sd)
505 of these values, given in permil (‰) relative to the IRMM-016 standard. Accuracy and external reproducibility were
506

518 assessed using seawater and USGS standard BCR-2, which gave $\delta^7\text{Li}$ values of $+31.3 \pm 0.6\text{‰}$ (2sd, n = 28) and
519 $+2.5 \pm 0.3\text{‰}$ (n = 5), respectively.

520 3.5.3. Neodymium isotopes and rare earth element concentrations

521 After decarbonation using 10% HCl for 30 min, clays were separated from decarbonated sediments into $<0.5 \mu\text{m}$
522 and $0.5\text{-}2 \mu\text{m}$ fractions (analytical protocol for size fraction separation reported in Jaimes-Gutierrez et al., 2024).
523 A total of 18 samples (8 in the $<0.5 \mu\text{m}$ size fraction and 10 in the $0.5\text{-}2 \mu\text{m}$ size fraction) were analysed for their
524 neodymium (Nd) isotopic composition and their Nd and samarium (Sm) concentrations. Aliquots of about 1.5 mg
525 of each clay fraction followed a sequential leaching procedure to remove Fe-Mn oxides and organic matter, based
526 on the protocol of Bayon et al. (2002) and Gutjahr et al. (2007), slightly adapted. The Fe-Mn oxides were removed
527 using a solution of 0.5 M hydroxylamine hydrochloride in 20% v/v acetic acid for 48h. Then, the organic matter
528 was removed with a 5% H_2O_2 solution for 48h.

529
530 The leached samples were dried and digested by alkaline fusion following the protocol of Bayon et al. (2009),
531 along with certified standards (BHVO-2, BRC-2) from the United States Geological Survey (USGS).
532 Approximately 50 mg of each sample underwent alkaline fusion in a carbon crucible with 0.6 g of NaOH and 1.2
533 g of Na_2O_2 heated at 650°C for 12 min in a furnace, before adding ultrapure water in which Fe-hydroxides
534 precipitated, concentrating rare earth elements. After centrifugation, the samples were dissolved in 3 ml 4 M HCl.

535
536 From this solution, an aliquot of 0.3 ml was extracted for analyses of Nd and Sm concentrations. Part of the
537 samples were measured for their Nd and Sm concentrations on an Agilent 7500 quadrupole ICP-MS spectrometer
538 in the Laboratoire Magmas et Volcans (LMV) in Clermont-Ferrand (France), and quantified using standard
539 bracketing with a solution of BHVO-2 during the session. Accuracy and reproducibility were assessed using two
540 BHVO-2 and one BCR-2 samples among the samples. Deviations of Nd and Sm concentrations from these
541 standards were below 11%. The other part of the samples was measured for their Nd and Sm concentrations on a
542 Thermo Scientific X-Series II® at the Pole Spectrométrie Océan in Brest (France), and quantified using multi-
543 element calibration standards prepared from single element standards purchased from SCP science (Baie d'Urfé,
544 Québec, Canada). Accuracy and reproducibility were assessed using one BHVO-2 and one BCR-2 sample, which
545 were analysed among the samples. Deviations of Nd and Sm concentrations from these standards were below 7
546 %.

547
548 Purified neodymium fractions were isolated from the mother solution by ion chromatography following the
549 protocol described in Gaitan et al. (2023) for the low-pressure, automated column chromatography PrepFAST-
550 MC® system device, using AG50W-X8 (200-400 mesh) resin for rare earth element separation and Ln Spec (50-
551 100 μm) resin for Nd separation. Part of the neodymium isotopic measurements was performed on a MC-ICP-MS
552 Neptune Plus (Thermo Scientific) at the Laboratoire Magmas et Volcans in Clermont-Ferrand (France). Ratios
553 were corrected for mass bias using an exponential law and a $^{143}\text{Nd}/^{144}\text{Nd}$ ratio of 0.7219. Mass-bias-corrected
554 $^{143}\text{Nd}/^{144}\text{Nd}$ were normalised to a JNdi-1 value of 0.512115 (Tanaka et al., 2000). Repeated measurements of
555 JNdi-1 throughout the session gave an external reproducibility of ± 0.000009 (2σ , n = 15), corresponding to \pm
556 0.18 in the standard $\epsilon_{\text{Nd}}(0)$ notation. Analyses of two BHVO-2 reference materials yielded a $^{143}\text{Nd}/^{144}\text{Nd}$ ratio of
557 0.512991 ± 0.000005 for each, in excellent agreement with the published value of 0.512990 ± 0.000010 (Weis et al.,
558 2005). The other part of the samples was analysed on an MC-ICP-MS Neptune Plus (Thermo Scientific) at the
559 ENS of Lyon (France). Ratios were corrected for mass bias using an exponential law and a $^{143}\text{Nd}/^{144}\text{Nd}$ ratio of
560 0.7219. Mass-bias-corrected $^{143}\text{Nd}/^{144}\text{Nd}$ values were normalised to a JNdi-1 value of 0.512115 (Tanaka et al.,
561 2000). Repeated measurements of JNdi-1 throughout the session gave an external reproducibility of ± 0.000018
562 (2σ , n = 16), corresponding to ± 0.34 in the standard $\epsilon_{\text{Nd}}(0)$ notation. Analyses of four BHVO-2 reference materials
563 gave an average $^{143}\text{Nd}/^{144}\text{Nd}$ ratio of 0.512985 ± 0.000009 for each, in agreement with the published value of
564 0.512990 ± 0.000010 (Weis et al., 2006).

565
566 The data are reported in the standard epsilon notation $\epsilon_{\text{Nd}} = [((^{143}\text{Nd}/^{144}\text{Nd})_{\text{sample}} / (^{143}\text{Nd}/^{144}\text{Nd})_{\text{CHUR}}) - 1] * 10^4$,
567 corrected for the radioactive decay of ^{147}Sm to ^{143}Nd based on the Nd and Sm concentrations measured for each
568 sample ($^{147}\text{Sm}/^{144}\text{Nd} = \text{Sm}/\text{Nd} * 0.6049$), an age of 55.8 Ma, and the ^{147}Sm radioactive decay constant λ ($6.54 \times$
569 10^{-12}y^{-1} ; Lugmair & Marti, 1977). The CHUR (CHondritic Uniform Reservoir) $^{143}\text{Nd}/^{144}\text{Nd}$ ratio was also
570 corrected using a $^{147}\text{Sm}/^{144}\text{Nd}$ ratio of 0.1960 and a present-day value of 0.512630 (Bouvier et al., 2008).

571

Deleted: is

Deleted: H

Deleted: during

Deleted: 4 M

Deleted: were

Deleted: ,

Deleted: close to

Deleted: s

Deleted: close to

Deleted: s

Deleted: ,

Deleted: an

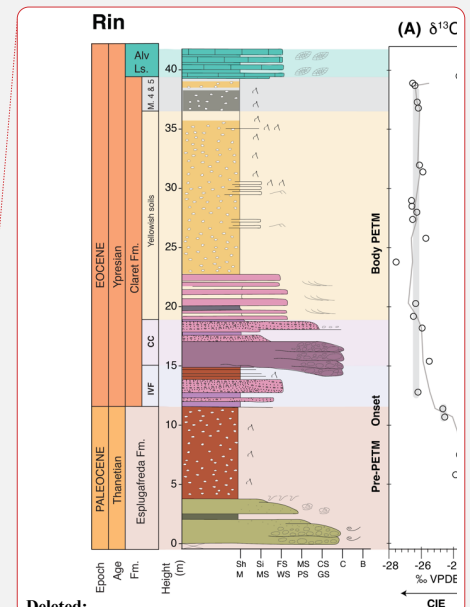
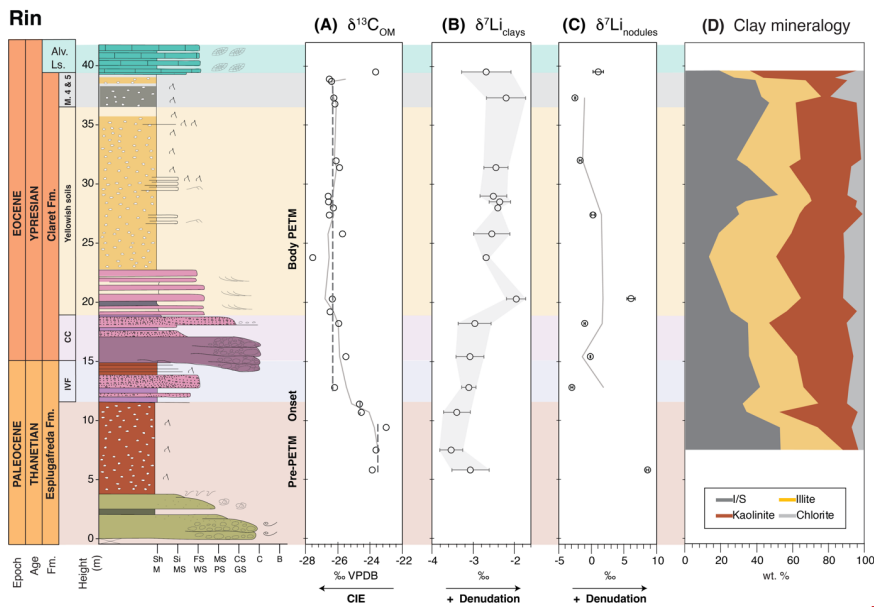
584 **4. Results**

585 **4.1. Clay mineralogy in the Rin section**

586 The clay mineralogy in the Rin section (Fig. 5D, Table S1) comprises mixed-layer illite-smectite (I/S), with a
 587 mean abundance of 34 ± 11 (1σ) wt.%; illite, 29 ± 9 wt.%; kaolinite, 30 ± 11 wt.%; and minor chlorite, 7 ± 5
 588 wt.%. The pre-PETM samples have a mixed-layer I/S abundance of 42 ± 10 %, decreasing to 32 ± 10 wt.% during
 589 the body of the PETM. The kaolinite abundance increases from 22 ± 14 wt.% to 32 ± 9 wt.% during the PETM
 590 body, while the illite and chlorite abundances remain stable.

591 **4.2. Organic matter carbon isotopes in the Rin section**

592 Throughout the section, the mean $\delta^{13}C_{OM}$ value is -25.7‰ , with a standard deviation (1σ) of 1.2‰ (Fig. 5A, Table
 593 S2). The pre-PETM samples, between 5.8 and 9.4 m, have a mean value of $-23.5 \pm 0.5\text{‰}$. A negative excursion
 594 begins in samples at 10.7 and 11.4 m, with values decreasing to $-24.6 \pm 0.1\text{‰}$. The most depleted values occur
 595 between 12.8 and 38.9 m, with a mean of $-26.3 \pm 0.5\text{‰}$. The final sample at 39.5 m, below the Alveolina
 596 Limestone, suggests a return to pre-PETM levels, with a value of -23.7‰ .
 597



598 **Figure 5. Rin section isotopes and clay mineralogy.** (A) The $\delta^{13}C_{OM}$ record shows the negative Carbon Isotope
 599 Excursion (CIE), with an onset before the Claret Conglomerate and sustained negative values until the Alveolina
 600 Limestone. (B) The CIE was accompanied by a positive excursion in lithium isotopes of the clays (δ^7Li_{clays}),
 601 reaching a 0.9‰ excursion in the Yellowish soils member. (C) Lithium isotopes in the carbonate nodules showed
 602 high variability and a less conclusive trend, suggesting clay contamination. (D) Rin section clay mineralogy. The
 603 pre-PETM and body intervals were determined based on the $\delta^{13}C_{OM}$ record and the stratigraphy. Grey bars in A
 604 represent average values for $\delta^{13}C_{OM}$ in the pre-PETM and in-PETM intervals, and in B they outline the analytical
 605 uncertainty ($2sd$) of δ^7Li_{clays} .
 606

607 **4.3. Lithium isotopes in the Rin and Esplugafreda sections**

608 The clays of the Rin section have a mean lithium isotope composition of $-2.9 \pm 0.5\text{‰}$ (1σ) (Fig. 5B, Table S2).
 609 Between 5.8 and 18.2 m, the mean composition is $-3.4 \pm 0.2\text{‰}$. Above this, from 20.3 to 39.5 m, the mean
 610 composition is $-2.6 \pm 0.2\text{‰}$, which corresponds to a shift towards more positive values of $\sim 0.8\text{‰}$. The minimum
 611 value of -3.7‰ is seen before the Claret Conglomerate, and the maximum value of -2.2‰ occurs immediately
 612 after the Claret Conglomerate, indicating a total range of up to $\sim 1.5\text{‰}$. The δ^7Li values measured on carbonate

616 nodules have a maximum value of 8.6‰, a minimum value of -3.0‰, and a mean composition of $0.9 \pm 4.0\%$
 617 (Fig. 5C). No clear temporal trend is observed in the $\delta^{7}\text{Li}_{\text{nodules}}$ record. No systematic correlation is observed
 618 between $\delta^{7}\text{Li}_{\text{clays}}$ and the relative abundance of individual clay minerals within analytical uncertainty (Fig. S1).

620 At the Esplugafreda section, the clays have a mean lithium isotope composition of $-3.7 \pm 0.7\%$ (Fig. 6B, Table
 621 S3). The pre-PETM samples (0-10 m and 21-28 m, Jaimes-Gutierrez et al., 2024 and references therein) have a
 622 mean composition of $-3.8 \pm 0.2\%$. The POE samples (~15–21 m) have a composition of $-3.2 \pm 0.2\%$, and the
 623 syn-PETM sediments have a composition of $-3.0 \pm 0.2\%$, indicating a PETM shift towards more positive values
 624 of $\sim 0.8\%$. The post-PETM sediments have a composition of $-4.5 \pm 0.4\%$. Samples from the pre-PETM, Pre-
 625 Onset Excursion (POE), and syn-PETM intervals display relatively heavier $\delta^{7}\text{Li}_{\text{clays}}$ values, whereas recovery-
 626 phase samples form a distinct cluster characterised by lighter $\delta^{7}\text{Li}_{\text{clays}}$ (Fig. S2).

628 **4.4. Neodymium isotopes in the Esplugafreda sections**

629 Throughout the Esplugafreda section, the 0.5–2 μm clays have a mean $\epsilon_{\text{Nd}}(t = 55.8 \text{ Ma})$ composition of $-10.94 \pm$
 630 $0.16 (2\sigma)$, while the $<0.5 \mu\text{m}$ fraction has a mean composition of -10.88 ± 0.11 (Fig. 6C, Table S4). In comparison,
 631 the typical analytical uncertainty on any individual sample measurement was $0.21 (2\sigma)$. Hence, these values are
 632 considered constant through time, with no deviation significantly outside the analytical uncertainty. The
 633 neodymium isotope measurements on the $<0.5 \mu\text{m}$ fraction are also indistinguishable from those on the 0.5–2 μm
 634 fraction (Fig. 6C).

Formatted ... [15]

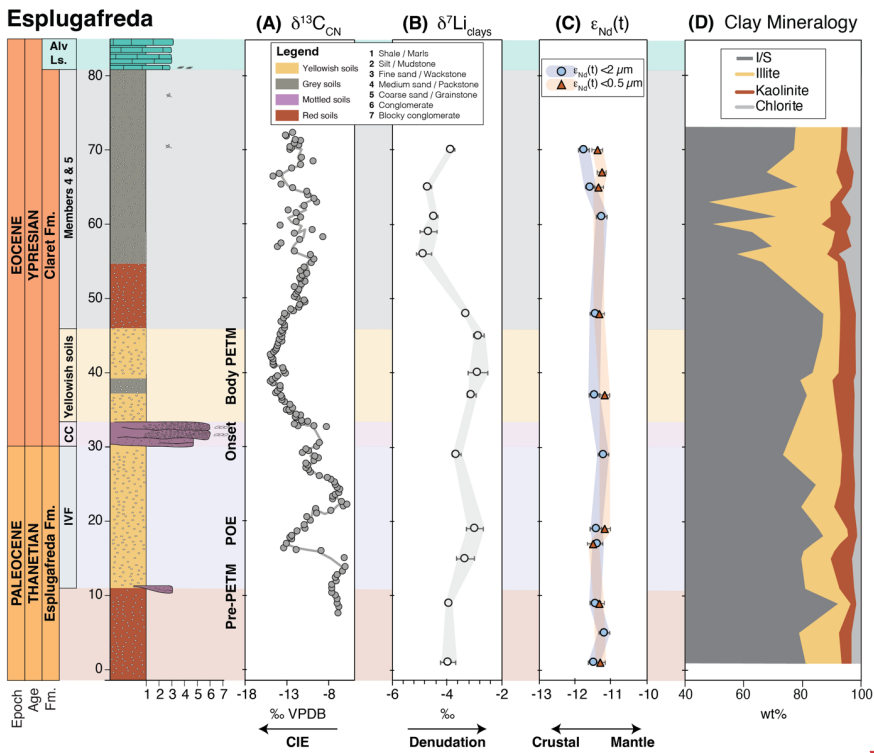
Deleted: 1

Formatted ... [16]

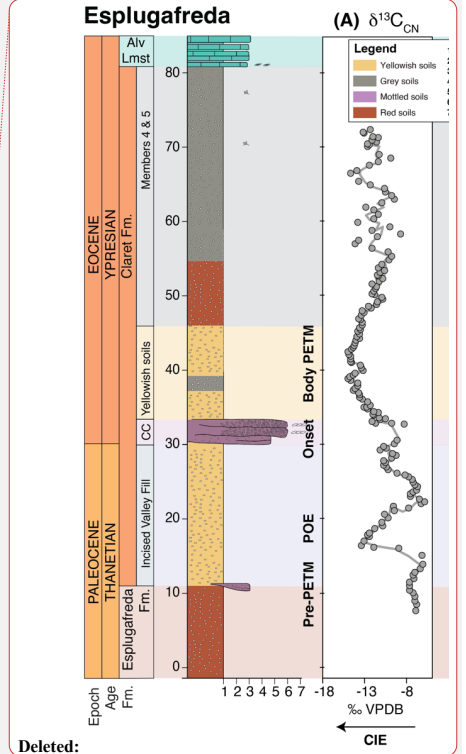
Deleted: The 0.5–2 μm clays throughout the Esplugafreda section ... have a mean $\epsilon_{\text{Nd}}(t = 55.8 \text{ Ma})$ composition of $-10.94 \pm 0.16 (2\sigma)$, while the $<0.5 \mu\text{m}$ fraction has ... a mean average...
 Deleted: 1

Formatted: English (US)

Deleted: Additional



637 **Figure 6.** Esplugafreda section isotopes and clay mineralogy. (A) The $\delta^{13}\text{C}$ record from microcrystalline
 638 carbonate nodules (from Khozyem, 2013) shows a negative carbon isotope excursion during the Pre-Onset
 639 Excursion (POE) and during the main body of the PETM. (B) There were positive excursions in lithium isotopes
 640 of the clays ($\delta^{7}\text{Li}_{\text{clays}}$) during both the POE and the main CIE of the PETM. (C) Neodymium isotopes ($\epsilon_{\text{Nd}}(t = 55.8$



Deleted:

657 *Ma*) show no variation throughout the section, indicating constant provenance. (D) Esplugafreda section clay
658 mineralogy (modified from Jaimes-Gutierrez et al., 2024).

659 5. Discussion

660 5.1. The PETM in the Rin section

661 The PETM sediments in the Rin section represent an archive of the climatic perturbation in a coastal terrestrial
662 setting (Pujalte et al., 2014; Prieur et al., 2025). This locality records a negative $\delta^{13}\text{C}_{\text{OM}}$ excursion of -2.8‰ from
663 pre- to syn-PETM (Fig. 5), in agreement with the CIE excursion of 3-5 ‰ identified in other southern Pyrenean
664 sections and other global settings (e.g. Schmitz et al., 2001; Schmitz and Pujalte, 2007; McInerney and Wing,
665 2011; Pujalte et al., 2015). The slightly reduced magnitude compared to the global record is consistent with
666 observed systematic differences in the CIE across different types of terrestrial archives, with paleosol carbonates
667 typically recording a 1-2 ‰ larger CIE than paleosol organic matter (Bowen et al., 2004; Cotton et al., 2015;
668 Gallagher et al., 2019). We do not identify the POE in the Rin section, and we suggest that it may have been
669 missed due to its occurrence further down in the section. Likewise, the recovery to pre-PETM values is also largely
670 absent, with just one sample below the Alevolina Limestone showing less depleted $\delta^{13}\text{C}_{\text{OM}}$ values.
671

672 The five members recognised in the Claret Fm. show an evolution from the eastern terrestrial setting into the
673 western marine domain. At Esplugafreda (Fig. 6), the five members are recorded (Basilici et al., 2022 and
674 references therein), including Member 1, IVF (pre-PETM); Member 2, the CC (Onset at Esplugafreda); Member
675 3, Yellowish soils (syn-PETM, or body of the PETM); Member 4, red paleosols with gypsum; and Member 5,
676 consisting of red mudstones with carbonate nodules (e.g. Schmitz and Pujalte, 2007; Baceta et al., 2011; Pujalte
677 et al., 2014; Colombera et al., 2017; Basilici et al., 2022). However, Member 4, the gypsum-rich member, only
678 occurs in the eastern part of the basin (Pujalte et al., 2014). Given the coastal position of the Rin section, at the
679 marine-continental transition and only ~20 km east of the Serraduy section, representing the westernmost
680 expression of the interfingering between continental deposits from the Esplugafreda Fm. and marine carbonates
681 (Prieur et al., 2025), the absence of Member 4 supports a further downstream position of the Rin section relative
682 to the Esplugafreda floodplain section.
683

684 Duller et al. (2019) estimated a lag time of approximately 16.5 ± 7.5 kyr between the CIE and the onset of coarse-
685 grained deposition at terrestrial sites in the Pyrenees. While sections such as Tendrui, Claret, and Campo (Pujalte
686 et al., 2009; Domingo et al., 2009) display a stratigraphic offset consistent with this lag, the Esplugafreda section
687 does not show such an offset (Duller et al., 2019). In the Rin section discussed here, we observe a clear offset
688 between the onset of the CIE and the arrival of coarse-grained sediments, specifically the Claret Conglomerate
689 (Fig. 5). To correctly position the lag time and explore the missing POE, future work could focus on high-
690 resolution $\delta^{13}\text{C}$ characterisation of the section.
691

692 The clay mineralogy at Rin further suggests a potential signal propagation effect. A shift from smectite-dominated
693 clays during the pre-PETM interval to an increase in kaolinite during the syn-PETM interval (Fig. 5D) could
694 indicate a transition to more hydrolysing conditions and to an increase in weathering intensity, or enhanced erosion
695 of former sedimentary formations rich in kaolinite. However, this trend also corresponds to a downstream
696 transition from authigenic smectite-rich paleosols at Esplugafreda (Fig. 6D) (e.g. Khozyem, 2013; Basilici et al.,
697 2022; Jaimes-Gutierrez et al., 2024) to kaolinite-dominated sediments in the Zumaia deep-marine section
698 (Gawenda et al., 1999; Schmitz et al., 2001; Bolle and Adatte, 2001). This mineralogical gradient from
699 Esplugafreda to Rin and Zumaia underscores the system connectivity across the basin (Pujalte et al., 2014).
700 However, such variations in clay composition may also reflect differences in sediment provenance (although
701 temporal changes are not observed in the ϵ_{Nd} record from Esplugafreda); differential mineral transport; enhanced
702 floodplain weathering; an increased proportion of eroded sedimentary formations downstream, bringing reworked
703 kaolinite (Pujalte et al., 2015); or a larger catchment area feeding the marine system (Chamley, 1989 and
704 references therein).
705

706 5.2. Evolution of weathering intensity in the continental realm of the Southern Pyrenees

707 Our $\delta^7\text{Li}_{\text{clays}}$ records from Rin and Esplugafreda both show a positive (~1‰) lithium isotope excursion in the
708 continental Southern Pyrenees during the onset and body of the PETM (Fig. 7). The $\delta^7\text{Li}$ values from carbonate
709 nodules at Rin show greater variability (Fig. 5C), but remain inconclusive due to potential clay contamination or
710 cation exchange between clays and carbonates (e.g. Pogge von Strandmann et al., 2019). Given the high Li content
711 in silicate minerals, even a minor clay particle content in the nodules could contaminate the carbonate signature.
712 Critically, the invariant ϵ_{Nd} composition of both size fractions throughout the Esplugafreda record (Fig. 6C)

Deleted: ,

Deleted: ,

Deleted: ,

Deleted: P

Deleted: ,

Formatted: English (UK)

Formatted: English (UK)

Deleted: ,

Deleted: ,

Deleted: ,

Moved down [1]: Marine and terrestrial $\delta^7\text{Li}$ records in both detrital and carbonate archives consistently show a negative excursion from pre-PETM to syn-PETM sediments. Pogge von Strandmann et al. (2021) documented a negative $\delta^7\text{Li}$ excursion of ~3‰ during the PETM in several marine carbonate sections and in detrital shales, indicating intensified global erosion rates (by 2–3×) and a 50–60% increase in silicate weathering fluxes, which was proposed to have contributed to climate stabilisation. Ramos et al. (2022) also found a negative $\delta^7\text{Li}_{\text{clays}}$ excursion, albeit with a smaller magnitude of ~1.5‰, in fine sediments of the Bighorn Basin, North America during the PETM, and this change was sustained during the recovery phase. Consistent with these results, Chen et al. (2023) found a negative $\delta^7\text{Li}_{\text{clays}}$ excursion of ~3‰ in the Nanyang Basin, which, together with the negative $\delta^7\text{Li}$ excursion in carbonates, was interpreted as recording a doubling of the regional silicate weathering intensity during the PETM.

Deleted: ¶

In contrast, our

Formatted: English (UK)

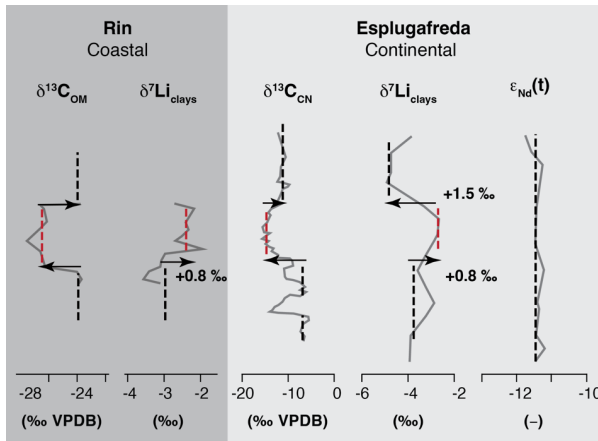
Deleted: the

Deleted: ,

Deleted: V

Deleted: the samples in

745 supports a constant provenance of the sediments, which suggests that the $\delta^7\text{Li}_{\text{clays}}$ records can be reliably
 746 interpreted as a reflection of weathering regime changes in response to the climatic perturbation.
 747



748 **Figure 7.** Comparison of isotopic results from the Rin and Esplugafreda sections. Grey solid lines show the raw
 749 data, while dashed black and red lines indicate typical values for different intervals, where red represents the
 750 PETM. The pre-PETM and post-PETM shifts are indicated with the black arrows, and the magnitudes of the
 751 $\delta^7\text{Li}_{\text{clays}}$ excursions are reported.
 752

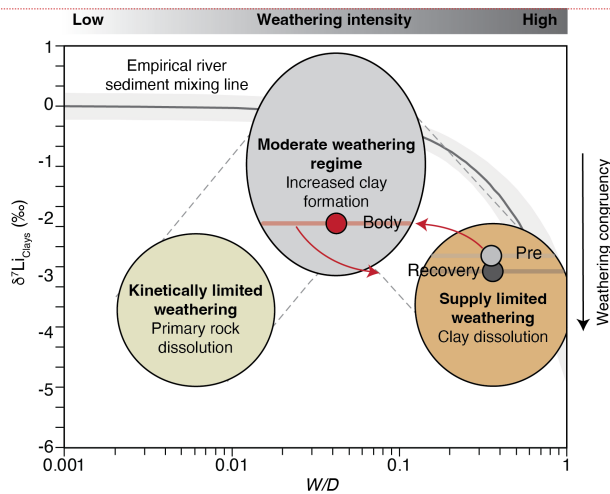
753 In many other PETM records, both marine and terrestrial $\delta^7\text{Li}$ values show a negative excursion from pre-PETM
 754 to syn-PETM conditions. Pogge von Strandmann et al. (2021) documented a negative $\delta^7\text{Li}$ excursion of $\sim 3\%$
 755 during the PETM in several marine carbonate sections and in detrital shales, indicating intensified global erosion
 756 rates (by 2–3 \times) and a 50–60% increase in silicate weathering fluxes, which was proposed to have contributed to
 757 climate stabilisation. Ramos et al. (2022) also found a negative $\delta^7\text{Li}_{\text{clays}}$ excursion, albeit with a smaller magnitude
 758 of $\sim 1.5\%$, in fine sediments of the Bighorn Basin, North America during the PETM, and this change was sustained
 759 during the recovery phase. Consistent with these results, Chen et al. (2023) found a negative $\delta^7\text{Li}_{\text{clays}}$ excursion of
 760 $\sim 3\%$ in the Nanyang Basin, East Asia, which, together with the negative $\delta^7\text{Li}$ excursion in the lacustrine
 761 carbonates, was interpreted as recording a doubling of the regional silicate weathering intensity during the PETM.
 762

763 Why, then, do the Southern Pyrenees floodplains record a positive $\delta^7\text{Li}_{\text{clays}}$ excursion during the PETM? We
 764 interpret the positive $\delta^7\text{Li}_{\text{clays}}$ excursion during the PETM as a shift towards increased incongruent weathering
 765 (moderate weathering regime), characterised by enhanced clay formation in the floodplain deposits. This regime
 766 would be characterised by increased chemical weathering, but relatively greater increases in physical erosion and
 767 sediment transport (e.g. Pujalte et al., 2015; Chen et al., 2018; Prieur et al., 2024), due to enhanced runoff causing
 768 short water residence times and rapid sediment export (i.e. lower W/D ; Fig. 8). Hydrological changes during the
 769 PETM are widely documented in the Southern Pyrenees (Schmitz and Pujalte, 2007; Pujalte et al., 2015; Chen et
 770 al., 2018; Rush et al., 2021; Prieur et al., 2024, 2025; Jaimes-Gutierrez et al., 2024) and likely played a central
 771 role in driving those weathering changes. A shift towards more intense, episodic rainfall, without an increase in
 772 mean annual precipitation (Rush et al., 2021), could have reduced infiltration, increased runoff, and shortened
 773 water–mineral interaction times. These processes would lead to decreased clay formation in the uplands by
 774 shortening water–rock interaction times (Kump et al., 2000; Riebe et al., 2004), while shifting clay production and
 775 accumulation towards lowland environments, where longer sediment residence times promote authigenic clay
 776 formation, consistent with modern river floodplain processes (e.g. Dellinger et al., 2015; Maffre et al., 2020). We
 777 also note that weathering processes are highly heterogeneous, and therefore global variability during the PETM
 778 can be expected (e.g. Frings, 2019). Critically, A decrease in W/D can lead both to positive or negative $\delta^7\text{Li}$
 779 excursions, depending on the starting weathering regime (Krause et al., 2023).
 780

781 Increasing evaporation, as recorded by gypsum lenses in Esplugafreda (Baceta et al., 2011; Khozyem, 2013;
 782 Jaimes-Gutierrez et al., 2024 and references therein), could also result in oversaturated pore waters, favouring
 783 clay formation. Experimental and field-based studies show that enhanced evaporation and reduced water
 784

- Formatted: Centred, Keep with next
- Deleted: /
- Deleted: and Rin
- Formatted: Font: (Default) Times New Roman, 10 pt, Bold, Font colour: Text 1
- Formatted: Font: (Default) Times New Roman, 10 pt, Font colour: Text 1
- Formatted: (... [18])
- Formatted: Font: (Default) Times New Roman, Font colour: Text 1
- Formatted: Caption
- Deleted: ,
- Deleted: with
- Formatted: Font: (Default) Times New Roman, Font colour: Text 1
- Formatted: (... [19])
- Deleted: form syn to PETM
- Formatted: English (UK)
- Moved (insertion) [1]
- Deleted: M...rine and terrestrial $\delta^7\text{Li}$ values show records in both detrital and carbonate archives consistently show...a negative excursion from pre-PETM to syn-PETM sedi (... [20])
- Formatted: (... [21])
- Deleted: ¶
- Formatted: English (UK)
- Formatted: (... [22])
- Formatted: Normal
- Deleted:Pujalte et al., 2015; Chen et al., 2018; Prieur et al., 2024), due to enhanced runoff causing short water residence times and rapid sediment export (i.e., (... [23])
- Deleted: 7... Hydrological changes during the PETM are widely documented in the Southern Pyrenees (Schmitz and Pujalte, 2007; Pujalte et al., 2015; Chen et al., 2018; Rush et al., 2021; Prieur et al., 2024, 2025; Jaimes-Gutierrez et al., 2024) and likely played a central role in driving those weathering changes. A shift towards more intense, episodic rainfall, without an increase in mean annual precipitation (Rush et al., 2021), could have reduced infiltration, increased runoff, and shortened water–mineral interaction times. These processes would lead to decreased clay formation in the uplands by shortening water–rock interaction times (Kump et al., 2000; Riebe et al., 2004), but increased...hile shifting clay production and accumulation in...owards lowland environments... (... [24])
- Formatted: Font: Italic
- Formatted: (... [25])
- Deleted: .
- Formatted: Font: 12 pt, Font colour: Auto, English (US)
- Deleted: which would

846 availability increase the dissolved $\delta^7\text{Li}$ values in soil and pore waters, leading to higher $\delta^7\text{Li}$ compositions of clays
 847 forming in equilibrium with these fluids (Xu et al., 2022; Pogge von Strandmann et al., 2023). Hydrological
 848 controls can also influence the $\delta^7\text{Li}_{\text{clays}}$ signatures by regulating water-rock interactions, sediment transport, and
 849 secondary mineral formation (Fig. 8). In supply-limited weathering regimes, increased runoff shortens water-
 850 rock interaction times and lowers dissolved $\delta^7\text{Li}$ values in river waters (Zhang et al., 2022), while enhanced
 851 sediment transfer promotes sediment storage and prolonged water-sediment interaction in floodplains, where
 852 continued clay alteration and isotopic re-equilibration can yield relatively higher $\delta^7\text{Li}$ values in the clay fraction
 853 preserved in lowland deposits. Overall, rapid sediment transport limits basin-scale weathering intensity, despite
 854 localised clay formation in floodplain environments.



856
 857 **Figure 8.** Weathering regime change from pre-PETM to syn-PETM based on $\delta^7\text{Li}_{\text{clays}}$ in the continental deposits
 858 of the Southern Pyrenees. The floodplain records were characterised by a decrease in weathering intensity and
 859 an increase in clay formation. Enhanced transport efficiency resulted in a major increase in physical erosion,
 860 with reaction kinetics limiting chemical weathering. Modified from Dellinger et al. (2015, 2017). At low W/D, the
 861 empirical river sediment mixing line includes the effects of mixing with primary minerals.

862 In the Esplugafreda section, the Recovery phase sees a shift towards more negative values than the pre-PETM
 863 conditions. During this interval, we observe a coeval increase in illite, kaolinite, and chlorite abundances in the
 864 Esplugafreda section Jaimes-Gutierrez et al. (2024). This shift in the clay mineral assemblage strongly suggests
 865 an increase in detrital input. For this reason, we consider that the observed excursion cannot be straightforwardly
 866 interpreted as a change in weathering intensity, but rather reflect the clay mineral assemblage (Fig. S2).

867
 868 Temperature effects on lithium isotope fractionation are minor in the Southern Pyrenees. While lithium isotope
 869 fractionation during clay formation is temperature-dependent (Vigier et al., 2008; Li and West, 2014), the
 870 fractionation factor (α) for incorporation in smectite is nearly constant across typical surface weathering
 871 temperatures (Vigier et al., 2008). Using the -3°C warming estimated for the continental Pyrenees across the
 872 PETM (Jaimes-Gutierrez et al., 2024), the maximum temperature-driven change in clay $\delta^7\text{Li}$ values is expected
 873 to be only a few tenths of a per mil (Li and West, 2014). This effect would shift clay $\delta^7\text{Li}$ values slightly towards
 874 heavier values and could therefore contribute marginally to the observed excursion, but it is insufficient to explain
 875 the full magnitude of the $\sim 1\text{‰}$ positive $\delta^7\text{Li}_{\text{clays}}$ shift observed in the records. Hence, climatic and hydrological
 876 processes, rather than direct temperature effects, must dominate the $\delta^7\text{Li}$ signal.

877
 878 The differences in $\delta^7\text{Li}$ values between river water and bedrock are controlled by the balance between lithium
 879 release by mineral dissolution and lithium removal by secondary mineral formation (Bouchez et al., 2013). The
 880 Southern Pyrenees during the PETM was a relatively high-erosion regime, such that physical erosion dominated,
 881 increasing the sediment supply and exposing fresh minerals (Schmitz and Pujalte, 2007; Pujalte et al., 2015, 2016;
 882 Chen et al., 2018; Prieur et al., 2024, 2025). When erosion exposes fresh minerals, weathering rates increase with

Deleted: s
 Formatted: ... [26]

Deleted: , with higher clay $\delta^7\text{Li}$ compositions reflecting equilibrium with the water composition ... ADDIN ZOTERO_ITEM CSL_CITATION {"citationID": "a1eht6vcigm", "properties": {"formattedCitation": "(Xu et al., 2022; Pogge von Strandmann et al., 2023)", "plainCitation": "(Xu et al., 2022; Pogge von Strandmann et al., 2023)", "noteIndex": 0}, "citationItems": [{"id": "9478", "ur... [27]

Deleted: excursion ... ignatures by regulating water-rock interactions, sediment transport, and secondary minera... [28]

Formatted: English (UK)

Deleted: ,

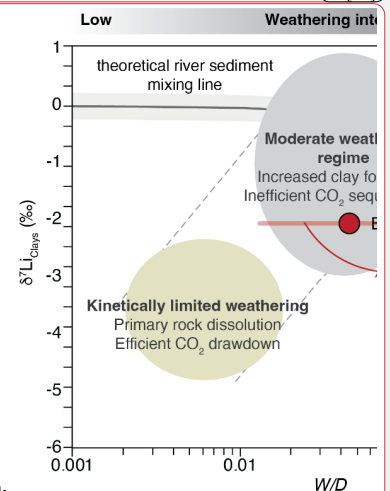
Formatted: English (UK)

Formatted: ... [29]

Deleted:

Formatted: ... [30]

Deleted: as faster runoff would result in less time for water-rock interaction, leading to less time for clay formatio... [31]



Deleted:

Deleted: theoretical

Deleted: Considering the mean annual air temperatures for the continental Pyrenees were a minimum of 23°C pr... [32]

Formatted: ... [33]

Deleted: the resulting maximum fractionation from pre-PETM to syn-PETM was -0.70‰

Formatted: ... [34]

Deleted: Although this fractionation towards more negative values may have had a small effect in reducing the ma... [35]

Deleted: s

Formatted: ... [36]

Field Code Changed

1109 total denudation, albeit less strongly than the increases in erosion, consistent with shared controls on chemical
1110 weathering and physical denudation rates (Riebe et al., 2004; West et al., 2005). Even though high-relief regions
1111 produce weakly weathered sediments, their high sediment yields and moderate clay formation rates result in
1112 elevated weathering fluxes (Gaillardet et al., 1999). Therefore, we propose that the Southern Pyrenean floodplains
1113 record a shift from a high-weathering intensity regime to a moderate-weathering intensity regime during the
1114 PETM (Fig. 8). The pre-PETM conditions were characterised by a low reactivity of the parent lithology (Kump
1115 and Arthur, 1997; Caves Rügenstein et al., 2019), associated with the carbonate-rich, reworked sediments in the
1116 floodplain deposits, and hence low total weathering fluxes. The above scenario is also consistent with the "system-
1117 clearing" event documented in western North America (Foreman et al., 2012), where sediment transport surged
1118 in response to rapid climatic forcing, as well as with other Eocene warming events such as the Mid-Eocene
1119 Climatic Optimum, which saw a shift towards enhanced clay formation and a lower weathering intensity (Krause
1120 et al., 2023).

Deleted: 7

1121
1122 The progressive increase in kaolinite content from Esplugafreda to Rin may reflect an evolving weathering signal
1123 during sediment transport from the hinterland towards the coastal plains, which potentially extended into the
1124 marine realm. This scenario supports a basin-wide connectivity between climate-driven terrestrial processes and
1125 marine sedimentary records. In addition, the increase in kaolinite content from Esplugafreda to Rin supports a
1126 shift in clay formation processes during the PETM. Kaolinite is typically associated with intense leaching and
1127 more advanced weathering, often forming under warm, humid, and periodically saturated conditions (Chamley,
1128 1989; Velde and Meunier, 2008). Hence, its enrichment suggests either intensified in-situ clay formation in the
1129 floodplains or increased transport of weathered material from the uplands to the lowlands. In either case, this shift
1130 implies greater clay mineral production, consistent with a more incongruent weathering regime driving the
1131 observed positive $\delta^7\text{Li}_{\text{clays}}$ excursion. Alternatively, enhanced kaolinite supply from the erosion-driven
1132 exhumation of older sediments cannot be ruled out based on the current evidence.

Deleted: A possible explanation for t

1133
1134 Despite these insights, key questions remain unresolved. In particular, a comprehensive study of the provenance
1135 and evolution of clay mineralogy is still needed to determine to what extent the observed patterns along the
1136 sediment routing system reflect changes in weathering intensity, differential mineral transport, or sediment
1137 reworking. Equally important is the need to constrain the precise age of the clay formation in relation to the timing
1138 of the different phases of the PETM, which is critical for reconstructing the temporal dynamics of the weathering
1139 regime in the Southern Pyrenees. Addressing these gaps will be crucial for better understanding how continental
1140 weathering systems responded to extreme climatic perturbations in the past and how they may behave under future
1141 global warming scenarios.

Formatted: English (UK)

1143 6. Conclusions

1144 We explored the silicate weathering response to the PETM in two terrestrial sections from the Tremp-Graus Basin
1145 of the Southern Pyrenees. These floodplain records show a positive $\delta^7\text{Li}_{\text{clays}}$ excursion, contrasting with the
1146 commonly observed global negative $\delta^7\text{Li}$ excursion in clays and carbonates. We interpret this excursion as
1147 reflecting a shift towards a moderate-intensity, incongruent weathering regime from an initial high-intensity,
1148 supply-limited regime. The high erosion rates associated with increased extreme rainfall events and channel
1149 mobility may have been the central factor influencing sediment residence times, with rapid sediment transport
1150 limiting the extent of chemical weathering. Nevertheless, the elevated denudation rates would have led to higher
1151 sediment and dissolved cation fluxes to the ocean, thereby enhancing regional CO_2 drawdown.

Deleted: conditions

1152 We explored two potential archives for recording continental weathering processes using lithium isotopes. The
1153 clay records show a distinct response, reflected in positive $\delta^7\text{Li}_{\text{clays}}$ excursions synchronous with the negative CIE.
1154 However, the $\delta^7\text{Li}_{\text{nodules}}$ signal recorded in the carbonate nodules is less conclusive, and we interpret the high
1155 temporal variability as a sign of potential contamination by clays in the nodules. Given that Li concentrations in
1156 silicate minerals are higher than in carbonates by several orders of magnitude, even minor amounts of clays could
1157 have resulted in a mixed response in the nodules. Future studies should explore weaker leaching approaches on
1158 such nodules and seek to validate such data with major and trace element analyses.

Deleted: strong

1160
1161 Provided coeval formation, the increase in kaolinite content from Esplugafreda to Rin provides mineralogical
1162 support for more hydrolysing conditions and clay formation during the PETM in the Tremp-Graus Basin,
1163 reinforcing the interpretation of more incongruent weathering under altered hydroclimatic conditions. Notably,
1164 the parent material in these floodplain paleosols is carbonate-rich and relatively unreactive. These results highlight
1165 the critical role of hydrological controls, especially rainfall intensity, runoff dynamics, and sediment residence
1166 time, in shaping continental weathering responses during extreme climate events.

1172 Finally, we propose that to fully quantify weathering dynamics during the PETM in the Southern Pyrenees, further
1173 work is needed to: (1) constrain the chronology of clay formation; (2) trace the evolution of clay mineralogy and
1174 provenance from source to sink; and (3) integrate continental and marine weathering records across the sediment
1175 routing system. Together, these steps will be essential for refining our understanding of weathering behaviour and
1176 the associated climate feedbacks under rapid climatic perturbations, and for improving predictions of Earth's
1177 surface processes in semi-arid floodplain systems in future global warming scenarios.

1179 **Acknowledgments**

1180 We acknowledge funding from the European Union's Horizon 2020 research and innovation programme under
1181 the Marie Skłodowska-Curie grant agreement No. 860383 S2S FUTURE. D.J.W. was supported by a NERC
1182 independent research fellowship (NE/T011440/1). We thank Justine Blondet for her support in neodymium
1183 isotope chromatography.

1184

1185 **Author contributions**

1186 R.J.G. performed sample collection, analytical work (clay mineralogy, RockEval, lithium and neodymium ion-
1187 exchange chromatography), data interpretation, visualisation, and original manuscript writing.

1188 M.P. contributed to sample collection, data interpretation, visualisation, and manuscript writing.

1189 D.J.W. and P.A.E.P.V.S. contributed to analytical work on lithium isotopes, data interpretation, and manuscript
1190 writing.

1191 E.P. conducted analytical work on neodymium isotopes, data interpretation, manuscript writing, and provided
1192 supervision.

1193 T.A. conducted RockEval analyses, contributed to data interpretation, manuscript writing, and provided
1194 supervision.

1195 J.E.S. conducted $\delta^{13}\text{C}$ analyses on organic matter and contributed to data interpretation and manuscript writing.

1196 S.C. acquired funding for the project, contributed to sample collection, data interpretation, and manuscript writing,
1197 and provided supervision.

1198

1199 **Conflict of interest**

1200 The authors declare that they have no conflict of interest relevant to this study.

1201

1202 **References**

1203 Adatte, T., Stinnesbeck, W., and Keller, G., 1996, Lithostratigraphic and mineralogic correlations of near K/T
1204 boundary clastic sediments in northeastern Mexico: Implications for origin and nature of deposition, *in*
1205 The Cretaceous-Tertiary Event and Other Catastrophes in Earth History, Geological Society of
1206 America, doi:10.1130/0-8137-2307-8.211.

1207 Anderson, S.P., Von Blanckenburg, F., and White, A.F., 2007, Physical and Chemical Controls on the Critical
1208 Zone: Elements, v. 3, p. 315–319, doi:10.2113/gselements.3.5.315.

1209 Baceta, J.I., Pujalte, V., and Bernaola, G., 2005, Paleocene corallgal reefs of the western Pyrenean basin,
1210 northern Spain: New evidence supporting an earliest Paleogene recovery of reefal ecosystems:
1211 Palaeogeography, Palaeoclimatology, Palaeoecology, v. 224, p. 117–143,
1212 doi:10.1016/j.palaeo.2005.03.033.

1213 Baceta, J.I., Pujalte, V., Wright, V.P., and Schmitz, B., 2011, Carbonate platform models, sea/ level changes and
1214 extreme climatic events during the Paleocene/ Eocene greenhouse interval: A basin-platform-coastal
1215 plain transect across the southern Pyrenean basin: 28th IAS Meeting of Sedimentology.

1216 Barefoot, E.A., Nittrouer, J.A., Foreman, B.Z., Hajek, E.A., Dickens, G.R., Baisden, T., and Toms, L., 2022,
1217 Evidence for enhanced fluvial channel mobility and fine sediment export due to precipitation
1218 seasonality during the Paleocene-Eocene thermal maximum: v. 50, p. 116–120, doi:10.1130/G49149.1.

1219 Basilici, G., Colombera, L., Soares, M.V.T., Arévalo, O.J., Mountney, N.P., Lorenzoni, P., de Souza Filho,
1220 C.R., Mesquita, Á.F., and Janočko, J., 2022, Variations from dry to aquatic conditions in Vertisols
1221 (Esplugafreda Formation, Eastern Pyrenees, Spain): Implications for late Paleocene climate change:
1222 Palaeogeography, Palaeoclimatology, Palaeoecology, v. 595, p. 110972,
1223 doi:10.1016/j.palaeo.2022.110972.

Deleted: and

- 1225 Bauer, K.K., Vennemann, T.W., and Gilg, H.A., 2016, Stable isotope composition of bentonites from the Swiss
1226 and Bavarian Freshwater Molasse as a proxy for paleoprecipitation: *Palaeogeography,*
1227 *Palaeoclimatology, Palaeoecology*, v. 455, p. 53–64, doi:10.1016/j.palaeo.2016.02.002.
- 1228 Bayon, G., Burton, K.W., Soulet, G., Vigier, N., Dennielou, B., Etoubleau, J., Ponzevera, E., German, C.R., and
1229 Nesbitt, R.W., 2009, Hf and Nd isotopes in marine sediments: Constraints on global silicate
1230 weathering: *Earth and Planetary Science Letters*, v. 277, p. 318–326, doi:10.1016/j.epsl.2008.10.028.
- 1231 Bayon, G., German, C.R., Boella, R.M., Milton, J.A., Taylor, R.N., and Nesbitt, R.W., 2002, An improved
1232 method for extracting marine sediment fractions and its application to Sr and Nd isotopic analysis:
1233 *Chemical Geology*, v. 187, p. 179–199, doi:10.1016/S0009-2541(01)00416-8.
- 1234 Behar, F., Beaumont, V., and De B. Penteado, H.L., 2001, Rock-Eval 6 Technology: Performances and
1235 Developments: *Oil & Gas Science and Technology*, v. 56, p. 111–134, doi:10.2516/ogst:2001013.
- 1236 Bolle, M.-P., and Adatte, T., 2001, Palaeocene- early Eocene climatic evolution in the Tethyan realm: clay
1237 mineral evidence: *Clay Minerals*, v. 36, p. 249–261, doi:10.1180/000985501750177979.
- 1238 Bouchez, J., Von Blanckenburg, F., and Schuessler, J.A., 2013, Modeling novel stable isotope ratios in the
1239 weathering zone: *American Journal of Science*, v. 313, p. 267–308, doi:10.2475/04.2013.01.
- 1240 Bouvier, A., Vervoort, J.D., and Patchett, P.J., 2008, The Lu–Hf and Sm–Nd isotopic composition of CHUR:
1241 Constraints from unequilibrated chondrites and implications for the bulk composition of terrestrial
1242 planets: *Earth and Planetary Science Letters*, v. 273, p. 48–57, doi:10.1016/j.epsl.2008.06.010.
- 1243 Bowen, G.J., Beerling, D.J., Koch, P.L., Zachos, J.C., and Quattlebaum, T., 2004, A humid climate state during
1244 the Palaeocene/Eocene thermal maximum: *Nature*, v. 432, p. 495–499, doi:10.1038/nature03115.
- 1245 Bufer, A., Hovius, N., Emberson, R., Rugenstein, J.K.C., Galy, A., Hassenruck-Gudipati, H.J., and Chang, J.-M.,
1246 2021, Co-variation of silicate, carbonate and sulfide weathering drives CO₂ release with erosion:
1247 *Nature Geoscience*, v. 14, p. 211–216, doi:10.1038/s41561-021-00714-3.
- 1248 Carmichael, M.J. et al., 2017, Hydrological and associated biogeochemical consequences of rapid global
1249 warming during the Paleocene-Eocene Thermal Maximum: *Global and Planetary Change*, v. 157, p.
1250 114–138, doi:10.1016/j.gloplacha.2017.07.014.
- 1251 Caves, J.K., Jost, A.B., Lau, K.V., and Maher, K., 2016, Cenozoic carbon cycle imbalances and a variable
1252 weathering feedback: *Earth and Planetary Science Letters*, v. 450, p. 152–163,
1253 doi:10.1016/j.epsl.2016.06.035.
- 1254 Caves Rugenstein, J.K., Ibarra, D.E., and von Blanckenburg, F., 2019, Neogene cooling driven by land surface
1255 reactivity rather than increased weathering fluxes: *Nature*, v. 571, p. 99–102, doi:10.1038/s41586-019-
1256 1332-y.
- 1257 Chamley, H., 1989, *Clay Sedimentology*: Berlin, Heidelberg, Springer Berlin Heidelberg, doi:10.1007/978-3-
1258 642-85916-8.
- 1259 Chen, Z., Ding, Z., Yang, S., Sun, J., Zhu, M., Xiao, Y., Tong, F., and Liang, Y., 2023, Strong Coupling
1260 Between Carbon Cycle, Climate, and Weathering During the Paleocene-Eocene Thermal Maximum:
1261 *Geophysical Research Letters*, v. 50, p. e2023GL102897, doi:10.1029/2023GL102897.
- 1262 Chen, C., Guertl, L., Foreman, B.Z., Hassenruck-Gudipati, H.J., Adatte, T., Honegger, L., Perret, M., Sluijs, A.,
1263 and Castellort, S., 2018, Estimating regional flood discharge during Palaeocene-Eocene global
1264 warming: *Scientific Reports*, v. 8, p. 13391, doi:10.1038/s41598-018-31076-3.
- 1265 Colombera, L., Arévalo, O.J., and Mountney, N.P., 2017, Fluvial-system response to climate change: The
1266 Paleocene-Eocene Tremp Group, Pyrenees, Spain: *Global and Planetary Change*, v. 157, p. 1–17,
1267 doi:10.1016/j.gloplacha.2017.08.011.

- 1268 Cotton, J.M., Sheldon, N.D., Hren, M.T., and Gallagher, T.M., 2015, Positive feedback drives carbon release
1269 from soils to atmosphere during Paleocene/Eocene warming: *American Journal of Science*, v. 315, p.
1270 337–361, doi:10.2475/04.2015.03.
- 1271 Dellinger, M., Bouchez, J., Gaillardet, J., Faure, L., and Moureau, J., 2017, Tracing weathering regimes using
1272 the lithium isotope composition of detrital sediments: *Geology*, v. 45, p. 411–414,
1273 doi:10.1130/G38671.1.
- 1274 Dellinger, M., Gaillardet, J., Bouchez, J., Calmels, D., Louvat, P., Dosseto, A., Gorge, C., Alanoca, L., and
1275 Maurice, L., 2015, Riverine Li isotope fractionation in the Amazon River basin controlled by the
1276 weathering regimes: *Geochimica et Cosmochimica Acta*, v. 164, p. 71–93,
1277 doi:10.1016/j.gca.2015.04.042.
- 1278 Dessert, C., Dupré, B., Gaillardet, J., François, L.M., and Allègre, C.J., 2003, Basalt weathering laws and the
1279 impact of basalt weathering on the global carbon cycle: *Chemical Geology*, v. 202, p. 257–273,
1280 doi:10.1016/j.chemgeo.2002.10.001.
- 1281 Dickens, G.R., O’Neil, J.R., Rea, D.K., and Owen, R.M., 1995, Dissociation of oceanic methane hydrate as a
1282 cause of the carbon isotope excursion at the end of the Paleocene: *Paleoceanography*, v. 10, p. 965–
1283 971, doi:10.1029/95PA02087.
- 1284 Domingo, L., López-Martínez, N., Leng, M.J., and Grimes, S.T., 2009, The Paleocene–Eocene Thermal
1285 Maximum record in the organic matter of the Claret and Tendryu continental sections (South-central
1286 Pyrenees, Lleida, Spain): *Earth and Planetary Science Letters*, v. 281, p. 226–237,
1287 doi:10.1016/j.epsl.2009.02.025.
- 1288 Dreyer, T., 1993, Quantified Fluvial Architecture in Ephemeral Stream Deposits of the Esplugafreda Formation
1289 (Palaeocene), Tremp-Graus Basin, Northern Spain, *in* Marzo, M. and Puigdefàbregas, C. eds., *Alluvial*
1290 *Sedimentation*, Wiley, p. 337–362, doi:10.1002/9781444303995.ch23.
- 1291 Duller, R.A., Armitage, J.J., Manners, H.R., Grimes, S., and Jones, T.D., 2019, Delayed sedimentary response
1292 to abrupt climate change at the Paleocene-Eocene boundary, northern Spain: *Geology*, v. 47, p. 159–
1293 162, doi:10.1130/G45631.1.
- 1294 Eichenseer, H., 1988, *Facies Geology Of Late Maestrichtian To Early Eocene Coastal And Shallow Marine*
1295 *Sediments (Tremp-Graus Basin, Northeastern Spain)*:
- 1296 Eichenseer, H., and Luterbacher, H., 1992, The marine paleogene of the tremp region (NE Spain)-depositional
1297 sequences, facies history, biostratigraphy and controlling factors: *Facies*, v. 27, p. 119–151,
1298 doi:10.1007/BF02536808.
- 1299 Espitalie, J., Deroo, G., and Marquis, F., 1985, La pyrolyse Rock-Eval et ses applications. Deuxième partie.:
1300 *Revue de l’Institut Français du Pétrole*, v. 40, p. 755–784, doi:10.2516/ogst:1985045.
- 1301 Foreman, B.Z., Heller, P.L., and Clementz, M.T., 2012, Fluvial response to abrupt global warming at the
1302 Palaeocene/Eocene boundary: *Nature*, v. 491, p. 92–95, doi:10.1038/nature11513.
- 1303 Frings, P.J., 2019, Palaeoweathering: How Do Weathering Rates Vary with Climate? *Elements*, v. 15, p. 259–
1304 265, doi:10.2138/gselements.15.4.259.
- 1305 Gaillardet, J., Dupré, B., and Allègre, C.J., 1999, Geochemistry of large river suspended sediments: silicate
1306 weathering or recycling tracer? *Geochimica et Cosmochimica Acta*, v. 63, p. 4037–4051,
1307 doi:10.1016/S0016-7037(99)00307-5.
- 1308 Gaitan, C.E., Pucéat, E., Pellenard, P., Blondet, J., Bayon, G., Adatte, T., Israel, C., Robin, C., and Guillocheau,
1309 F., 2023, Late Cretaceous erosion and chemical weathering record in the offshore Cape Basin: Source-
1310 to-sink system from Hf Nd isotopes and clay mineralogy: *Marine Geology*, v. 466, p. 107187,
1311 doi:10.1016/j.margeo.2023.107187.

- 1312 Gallagher, T.M., Cacciatore, C.G., and Breecker, D.O., 2019, Interpreting the Difference in Magnitudes of
1313 PETM Carbon Isotope Excursions in Paleosol Carbonate and Organic Matter: Oxidation of Methane in
1314 Soils Versus Elevated Soil Respiration Rates: *Paleoceanography and Paleoclimatology*, v. 34, p. 2113–
1315 2128, doi:10.1029/2019PA003596.
- 1316 Gawenda, P., Winkler, W., Schmitz, B., and Adatte, T., 1999, Climate and bioproductivity control on carbonate
1317 turbidite sedimentation (Paleocene to earliest Eocene, Gulf of Biscay, Zumaia, Spain): *Journal of*
1318 *Sedimentary Research*, v. 69, p. 1253–1261, doi:10.2110/jsr.69.1253.
- 1319 Gibbs, 1977, Clay Mineral Segregation in the Marine Environment: *SEPM Journal of Sedimentary Research*, v.
1320 Vol. 47, doi:10.1306/212F713A-2B24-11D7-8648000102C1865D.
- 1321 Godd ris, Y., Donnadi u, Y., Tombozafy, M., and Dessert, C., 2008, Shield effect on continental weathering:
1322 Implication for climatic evolution of the Earth at the geological timescale: *Geoderma*, v. 145, p. 439–
1323 448, doi:10.1016/j.geoderma.2008.01.020.
- 1324 G mez-Gras, D., Roig , M., Fondevilla, V., Oms, O., Boya, S., and Remacha, E., 2016, Provenance constraints
1325 on the Tremp Formation paleogeography (southern Pyrenees): Ebro Massif VS Pyrenees sources:
1326 *Cretaceous Research*, v. 57, p. 414–427, doi:10.1016/j.cretres.2015.09.010.
- 1327 Gutjahr, M., Frank, M., Stirling, C.H., Klemm, V., Van De Fliedert, T., and Halliday, A.N., 2007, Reliable
1328 extraction of a deepwater trace metal isotope signal from Fe–Mn oxyhydroxide coatings of marine
1329 sediments: *Chemical Geology*, v. 242, p. 351–370, doi:10.1016/j.chemgeo.2007.03.021.
- 1330 Hessler, A.M., Zhang, J., Covault, J., and Ambrose, W., 2017, Continental weathering coupled to Paleogene
1331 climate changes in North America: *Geology*, v. 45, p. 911–914, doi:10.1130/G39245.1.
- 1332 Hilton, R.G., 2023, Earth’s persistent thermostat: *Science*, v. 379, p. 329–330, doi:10.1126/science.adf3379.
- 1333 Jaimes-Gutierrez, R., Adatte, T., Puc at, E., Vennemann, T., Prieur, M., Wild, A.L., Khozyem, H., Vaucher, R.,
1334 and Castellort, S., 2024, Deciphering Paleocene-Eocene Thermal Maximum Climatic Dynamics:
1335 Insights From Oxygen and Hydrogen Isotopes in Clay Minerals of Paleosols From the Southern
1336 Pyrenees: *Paleoceanography and Paleoclimatology*, v. 39, p. e2024PA004858,
1337 doi:10.1029/2024PA004858.
- 1338 Jaimes-Gutierrez, R., Vimperc, L., Wilson, D.J., Blaser, P., Adatte, T., Sahoo, S., and Castellort, S., 2025a,
1339 Lithium isotopes reveal enhanced weathering fluxes in North America during the Paleocene–Eocene
1340 Thermal Maximum: *Geology*, doi:https://doi.org/10.1130/G53708.1.
- 1341 Jones, M.T. et al., 2023, Tracing North Atlantic volcanism and seaway connectivity across the Paleocene–
1342 Eocene Thermal Maximum (PETM): *Climate of the Past*, v. 19, p. 1623–1652, doi:10.5194/cp-19-
1343 1623-2023.
- 1344 Kennett, J.P., and Stott, L.D., 1991, Abrupt deep-sea warming, palaeoceanographic changes and benthic
1345 extinctions at the end of the Palaeocene: *Nature*, v. 353, p. 225–229, doi:10.1038/353225a0.
- 1346 Khozyem, H.M.A., 2013, Sedimentology, geochemistry and mineralogy of the Paleocene Eocene Thermal
1347 Maximum (PETM): Sediment records from Egypt, India and Spain [Doctoral Dissertation]: Universit 
1348 de Lausanne, 195 p.
- 1349 Kısak rek, B., James, R.H., and Harris, N.B.W., 2005, Li and $\delta^7\text{Li}$ in Himalayan rivers: Proxies for silicate
1350 weathering? *Earth and Planetary Science Letters*, v. 237, p. 387–401, doi:10.1016/j.epsl.2005.07.019.
- 1351 Krause, A.J., Sluijs, A., Van Der Ploeg, R., Lenton, T.M., and Pogge Von Strandmann, P.A.E., 2023, Enhanced
1352 clay formation key in sustaining the Middle Eocene Climatic Optimum: *Nature Geoscience*, v. 16, p.
1353 730–738, doi:10.1038/s41561-023-01234-y.
- 1354 Kump, L.R., and Arthur, M.A., 1997, Global Chemical Erosion during the Cenozoic: Weatherability Balances
1355 the Budgets, *in* Ruddiman, W.F. ed., *Tectonic Uplift and Climate Change*, Boston, MA, Springer US,
1356 p. 399–426, doi:10.1007/978-1-4615-5935-1_18.

- 1357 Kump, L.R., Brantley, S.L., and Arthur, M.A., 2000, Chemical Weathering, Atmospheric CO₂, and Climate:
1358 Annual Review of Earth and Planetary Sciences, v. 28, p. 611–667,
1359 doi:10.1146/annurev.earth.28.1.611.
- 1360 Li, G., and West, A.J., 2014, Evolution of Cenozoic seawater lithium isotopes: Coupling of global denudation
1361 regime and shifting seawater sinks: Earth and Planetary Science Letters, v. 401, p. 284–293,
1362 doi:10.1016/j.epsl.2014.06.011.
- 1363 Liu, C.-Y., Wilson, D.J., Hathorne, E.C., Xu, A., and Pogge Von Strandmann, P.A.E., 2023, The influence of
1364 river-derived particles on estuarine and marine elemental cycles: Evidence from lithium isotopes:
1365 Geochimica et Cosmochimica Acta, v. 361, p. 183–199, doi:10.1016/j.gca.2023.08.015.
- 1366 Maffre, P., Godd ris, Y., Vigier, N., Moquet, J.-S., and Carretier, S., 2020, Modelling the riverine $\delta^7\text{Li}$
1367 variability throughout the Amazon Basin: Chemical Geology, v. 532, p. 119336,
1368 doi:10.1016/j.chemgeo.2019.119336.
- 1369 Maher, K., and Von Blanckenburg, F., 2023, The circular nutrient economy of terrestrial ecosystems and the
1370 consequences for rock weathering: Frontiers in Environmental Science, v. 10, p. 1066959,
1371 doi:10.3389/fenvs.2022.1066959.
- 1372 Mattauer, M., and Henry, J., 1974, Pyrenees: Special Publications, v. 4, no.1, p. 3–21.
- 1373 McInerney, F.A., and Wing, S.L., 2011, The Paleocene-Eocene Thermal Maximum: A Perturbation of Carbon
1374 Cycle, Climate, and Biosphere with Implications for the Future: Annual Review of Earth and Planetary
1375 Sciences, v. 39, p. 489–516, doi:10.1146/annurev-earth-040610-133431.
- 1376 Misra, S., and Froelich, P.N., 2012, Lithium Isotope History of Cenozoic Seawater: Changes in Silicate
1377 Weathering and Reverse Weathering: Science, v. 335, p. 818–823, doi:10.1126/science.1214697.
- 1378 Moore, D.M., and Reynolds, R.C., 1992, Moore, Reynolds 1997_X-Ray Diffraction.pdf: New York, Oxford
1379 University Press, 401 p.
- 1380 Moulton, K.L., West, J., and Berner, R.A., 2000, Solute flux and mineral mass balance approaches to the
1381 quantification of plant effects on silicate weathering: v. 300, p. 539–570.
- 1382 Mu oz, J.A., 1992, Evolution of a continental collision belt: ECORS-Pyrenees crustal balanced cross-section, *in*
1383 McClay, K.R. ed., Thrust Tectonics, Dordrecht, Springer Netherlands, p. 235–246, doi:10.1007/978-
1384 94-011-3066-0_21.
- 1385 Murray, J., and Jagoutz, O., 2024, Palaeozoic cooling modulated by ophiolite weathering through organic
1386 carbon preservation: Nature Geoscience, v. 17, p. 88–93, doi:10.1038/s41561-023-01342-9.
- 1387 Pistiner, J.S., and Henderson, G.M., 2003, Lithium-isotope fractionation during continental weathering
1388 processes: Earth and Planetary Science Letters, v. 214, p. 327–339, doi:10.1016/S0012-
1389 821X(03)00348-0.
- 1390 Pogge von Strandmann, P.A.E., Cosford, L.R., Liu, C.-Y., Liu, X., Krause, A.J., Wilson, D.J., He, X., McCoy-
1391 West, A.J., Gislason, S.R., and Burton, K.W., 2023, Assessing hydrological controls on the lithium
1392 isotope weathering tracer: Chemical Geology, v. 642, p. 121801, doi:10.1016/j.chemgeo.2023.121801.
- 1393 Pogge Von Strandmann, P.A.E., Fraser, W.T., Hammond, S.J., Tarbuck, G., Wood, I.G., Oelkers, E.H., and
1394 Murphy, M.J., 2019, Experimental determination of Li isotope behaviour during basalt weathering:
1395 Chemical Geology, v. 517, p. 34–43, doi:10.1016/j.chemgeo.2019.04.020.
- 1396 Pogge von Strandmann, P.A.E., Jenkyns, H.C., and Woodfine, R.G., 2013, Lithium isotope evidence for
1397 enhanced weathering during Oceanic Anoxic Event 2: Nature Geoscience, v. 6, p. 668–672,
1398 doi:10.1038/ngeo1875.

- 1399 Pogge von Strandmann, P.A.E., Jones, M.T., West, A.J., Murphy, M.J., Stokke, E.W., Tarbuck, G., Wilson,
1400 D.J., Pearce, C.R., and Schmidt, D.N., 2021, Lithium isotope evidence for enhanced weathering and
1401 erosion during the Paleocene-Eocene Thermal Maximum: *Science Advances*, v. 7, p. eabh4224,
1402 doi:10.1126/sciadv.abh4224.
- 1403 Pogge von Strandmann, P.A.E., Kasemann, S.A., and Wimpenny, J.B., 2020, Lithium and Lithium Isotopes in
1404 Earth's Surface Cycles: v. 16, p. 253–258, doi:10.2138/gselements.16.4.253.
- 1405 Porder, S., 2019, How Plants Enhance Weathering and How Weathering is Important to Plants: *Elements*, v. 15,
1406 p. 241–246, doi:10.2138/gselements.15.4.241.
- 1407 Prieur, M. et al., 2025, Climate Control on Erosion: Evolution of Sediment Flux From Mountainous Catchments
1408 During a Global Warming Event, PETM, Southern Pyrenees, Spain: *Geophysical Research Letters*, v.
1409 52, p. e2024GL112404, doi:10.1029/2024GL112404.
- 1410 Prieur, M., Whittaker, A.C., Nuriel, P., Jaimes-Gutierrez, R., Garzanti, E., Roigé, M., Somme, T.O.,
1411 Schlunegger, F., and Castelltort, S., 2024, Fingerprinting enhanced floodplain reworking during the
1412 Paleocene–Eocene Thermal Maximum in the Southern Pyrenees (Spain): Implications for channel
1413 dynamics and carbon burial: *Geology*, v. 52, p. 651–655, doi:10.1130/G52180.1.
- 1414 Puigdefbregas, C., and Souquet, P., 1986, Tecto-sedimentary cycles and depositional sequences of the Mesozoic
1415 and Tertiary from the Pyrenees: v. 129, p. 173–203.
- 1416 Pujalte, V., Baceta, J.I., and Schmitz, B., 2015, A massive input of coarse-grained siliciclastics in the Pyrenean
1417 Basin during the PETM: the missing ingredient in a coeval abrupt change in hydrological regime:
1418 *Climate of the Past*, v. 11, p. 1653–1672, doi:10.5194/cp-11-1653-2015.
- 1419 Pujalte, V., Robador, A., Aitor Payros, and Samsó, J.M., 2016, A siliciclastic braid delta within a lower
1420 Paleogene carbonate platform (Ordessa-Monte Perdido National Park, southern Pyrenees, Spain):
1421 Record of the Paleocene–Eocene Thermal Maximum perturbation: *Palaeogeography,
1422 Palaeoclimatology, Palaeoecology*, v. 459, p. 453–470, doi:10.1016/j.palaeo.2016.07.029.
- 1423 Pujalte, V., and Schmitz, B., 2005, Revisión de la estratigrafía del Grupo Tremp («Garumniense», Cuenca de
1424 Tremp-Graus, Pirineos meridionales):
- 1425 Pujalte, V., Schmitz, B., and Baceta, J.I., 2014, Sea-level changes across the Paleocene–Eocene interval in the
1426 Spanish Pyrenees, and their possible relationship with North Atlantic magmatism: *Palaeogeography,
1427 Palaeoclimatology, Palaeoecology*, v. 393, p. 45–60, doi:10.1016/j.palaeo.2013.10.016.
- 1428 Pujalte, V., Schmitz, B., Baceta, J.I., Orue-Etxebarria, X., Bernaola, G., Dinarès-Turell, J., Payros, A.,
1429 Apellaniz, E., and Caballero, F., 2009, Correlation of the Thanetian-Ilerdian turnover of larger
1430 foraminifera and the Paleocene-Eocene thermal maximum: confirming evidence from the Campo area
1431 (Pyrenees, Spain): *Geologica Acta*, v. 7.
- 1432 Ramos, E.J. et al., 2024, Competition or collaboration: Clay formation sets the relationship between silicate
1433 weathering and organic carbon burial in soil: *Earth and Planetary Science Letters*, v. 628, p. 118584,
1434 doi:10.1016/j.epsl.2024.118584.
- 1435 Ramos, E.J. et al., 2022, Swift Weathering Response on Floodplains During the Paleocene-Eocene Thermal
1436 Maximum: *Geophysical Research Letters*, v. 49, doi:10.1029/2021GL097436.
- 1437 Raymo, M.E., and Ruddiman, W.F., 1992, Tectonic forcing of late Cenozoic climate: *Nature*, v. 359, p. 117–
1438 122, doi:10.1038/359117a0.
- 1439 Riebe, C.S., Kirchner, J.W., and Finkel, R.C., 2004, Erosional and climatic effects on long-term chemical
1440 weathering rates in granitic landscapes spanning diverse climate regimes: *Earth and Planetary Science
1441 Letters*, v. 224, p. 547–562, doi:10.1016/j.epsl.2004.05.019.

- 1442 Roest, W.R., and Srivastava, S.P., 1991, Kinematics of the plate boundaries between Eurasia, Iberia, and Africa
1443 in the North Atlantic from the Late Cretaceous to the present: *Geology*, v. 19, p. 613,
1444 doi:10.1130/0091-7613(1991)019<0613:KOTPB>2.3.CO;2.
- 1445 Rosenbaum, G., Lister, G.S., and Duboz, C., 2002, Reconstruction of the tectonic evolution of the western
1446 Mediterranean since the Oligocene: *Journal of the Virtual Explorer*, v. 08,
1447 doi:10.3809/jvirtex.2002.00053.
- 1448 Roure, F., Choukroune, P., Berastegui, X., Munoz, J.A., Villien, A., Matheron, P., Bareyt, M., Seguret, M.,
1449 Camara, P., and Deramond, J., 1989, Ecorep deep seismic data and balanced cross sections: Geometric
1450 constraints on the evolution of the Pyrenees: *Tectonics*, v. 8, p. 41–50, doi:10.1029/TC008i001p00041.
- 1451 Rush, W.D., Kiehl, J.T., Shields, C.A., and Zachos, J.C., 2021, Increased frequency of extreme precipitation
1452 events in the North Atlantic during the PETM: Observations and theory: *Palaeogeography,*
1453 *Palaeoclimatology, Palaeoecology*, v. 568, p. 110289, doi:10.1016/j.palaeo.2021.110289.
- 1454 Rush, W., Zachos, J., Blackburn, T., and Pogge Von Strandmann, P.A.E., 2025, Continuous Sediment Sourcing
1455 and Changes in Weathering During the PETM in the Salisbury Embayment: *Paleoceanography and*
1456 *Paleoclimatology*, v. 40, p. e2025PA005116, doi:10.1029/2025PA005116.
- 1457 Schmitz, B., and Pujalte, V., 2007, Abrupt increase in seasonal extreme precipitation at the Paleocene-Eocene
1458 boundary: *Geology*, v. 35, p. 215, doi:10.1130/G23261A.1.
- 1459 Schmitz, B., and Pujalte, V., 2003, Sea-level, humidity, and land-erosion records across the initial Eocene
1460 thermal maximum from a continental-marine transect in northern Spain: *Geology*, v. 31, p. 689,
1461 doi:10.1130/G19527.1.
- 1462 Schmitz, B., Pujalte, V., and Nunhez-Betelu, K., 2001, Climate and sea-level perturbations during the Initial
1463 Eocene Thermal Maximum: evidence from siliciclastic units in the Basque Basin (Ermua, Zumaia and
1464 Trabakua Pass), northern Spain: *Palaeogeography, Palaeoclimatology, Palaeoecology* 165, p. 299–320.
- 1465 Spangenberg, J.E., 2006, Hydrocarbon Biomarkers in the Topla-Mezica Zinc-Lead Deposits, Northern
1466 Karavanke/Drau Range, Slovenia: *Paleoenvironment at the Site of Ore Formation*:
- 1467 Spangenberg, J.E., and Zufferey, V., 2019, Carbon isotope compositions of whole wine, wine solid residue, and
1468 wine ethanol, determined by EA/IRMS and GC/C/IRMS, can record the wine water status—a
1469 comparative reappraisal: *Analytical and Bioanalytical Chemistry*, v. 411, p. 2031–2043,
1470 doi:10.1007/s00216-019-01625-4.
- 1471 Tanaka, T. et al., 2000, JNdi-1: a neodymium isotopic reference in consistency with LaJolla neodymium:
1472 *Chemical Geology*, v. 168, p. 279–281, doi:10.1016/S0009-2541(00)00198-4.
- 1473 Teixell, A., Labaume, P., and Lagabrielle, Y., 2016, The crustal evolution of the west-central Pyrenees revisited:
1474 Inferences from a new kinematic scenario: *Comptes Rendus. Géoscience*, v. 348, p. 257–267,
1475 doi:10.1016/j.crte.2015.10.010.
- 1476 Tofelde, S., Bernhardt, A., Guerit, L., and Romans, B.W., 2021, Times Associated With Source-to-Sink
1477 Propagation of Environmental Signals During Landscape Transience: *Frontiers in Earth Science*, v. 9,
1478 p. 628315, doi:10.3389/feart.2021.628315.
- 1479 Tremblin, M. et al., 2022, Mercury enrichments of the Pyrenean foreland basins sediments support enhanced
1480 volcanism during the Paleocene-Eocene thermal maximum (PETM): *Global and Planetary Change*, v.
1481 212, p. 103794, doi:10.1016/j.gloplacha.2022.103794.
- 1482 Velde, B., and Meunier, A., 2008, *The Origin of Clay Minerals in Soils and Weathered Rocks*: Berlin,
1483 Heidelberg, Springer Berlin Heidelberg, doi:10.1007/978-3-540-75634-7.
- 1484 Vigier, N., Decarreau, A., Millot, R., Carignan, J., Petit, S., and France-Lanord, C., 2008, Quantifying Li
1485 isotope fractionation during smectite formation and implications for the Li cycle: *Geochimica et*
1486 *Cosmochimica Acta*, v. 72, p. 780–792, doi:10.1016/j.gca.2007.11.011.

1487 Vimpere, L. et al., 2023, Carbon isotope and biostratigraphic evidence for an expanded Paleocene–Eocene
1488 Thermal Maximum sedimentary record in the deep Gulf of Mexico: *Geology*, doi:10.1130/G50641.1.

1489 Walker, J.C.G., Hays, P.B., and Kasting, J.F., 1981, A negative feedback mechanism for the long-term
1490 stabilization of Earth’s surface temperature: *Journal of Geophysical Research: Oceans*, v. 86, p. 9776–
1491 9782, doi:10.1029/JC086iC10p09776.

1492 Wei, G.-Y., Pohl, A., Jiang, S., Zhang, H., Wang, W., A. E. Pogge Von Strandmann, P., Maffre, P., Xiong, G.,
1493 Shen, S., and Zhang, F., 2025, Changes in continental weathering regimes inhibited global marine
1494 deoxygenation during the Paleocene-Eocene thermal maximum: *Nature Communications*, v. 16, p.
1495 9163, doi:10.1038/s41467-025-64217-0.

1496 Weis, D., Kieffer, B., Maerschalk, C., Pretorius, W., and Barling, J., 2005, High-precision Pb-Sr-Nd-Hf isotopic
1497 characterization of USGS BHVO-1 and BHVO-2 reference materials: *Geochemistry, Geophysics,
1498 Geosystems*, v. 6, p. 2004GC000852, doi:10.1029/2004GC000852.

1499 West, A., Galy, A., and Bickle, M., 2005, Tectonic and climatic controls on silicate weathering: *Earth and
1500 Planetary Science Letters*, v. 235, p. 211–228, doi:10.1016/j.epsl.2005.03.020.

1501 Westerhold, T., Röhl, U., McCarren, H.K., and Zachos, J.C., 2009, Latest on the absolute age of the Paleocene–
1502 Eocene Thermal Maximum (PETM): New insights from exact stratigraphic position of key ash layers
1503 +19 and –17: *Earth and Planetary Science Letters*, v. 287, p. 412–419, doi:10.1016/j.epsl.2009.08.027.

1504 Wilson, D.J., Pogge von Strandmann, P.A.E., White, J., Tarbuck, G., Marca, A.D., Atkinson, T.C., and Hopley,
1505 P.J., 2021, Seasonal variability in silicate weathering signatures recorded by Li isotopes in cave drip-
1506 waters: *Geochimica et Cosmochimica Acta*, v. 312, p. 194–216, doi:10.1016/j.gca.2021.07.006.

1507 Winnick, M.J., Druhan, J.L., and Maher, K., 2022, Weathering intensity and lithium isotopes: A reactive
1508 transport perspective: *American Journal of Science*, v. 322, p. 647–682, doi:10.2475/05.2022.01.

1509 Xu, Z., Li, T., Li, G., Hedding, D.W., Wang, Y., Gou, L.-F., Zhao, L., and Chen, J., 2022, Lithium isotopic
1510 composition of soil pore water: Responses to evapotranspiration: *Geology*, v. 50, p. 194–198,
1511 doi:10.1130/G49366.1.

1512 Zachos, J.C., Dickens, G.R., and Zeebe, R.E., 2008, An early Cenozoic perspective on greenhouse warming and
1513 carbon-cycle dynamics: *Nature*, v. 451, p. 279–283, doi:10.1038/nature06588.

1514 Zachos, J.C., Wara, M.W., Bohaty, S., Delaney, M.L., Petrizzo, M.R., Brill, A., Bralower, T.J., and Premoli-
1515 Silva, I., 2003, A Transient Rise in Tropical Sea Surface Temperature During the Paleocene-Eocene
1516 Thermal Maximum: *Science*, v. 302, p. 1551–1554, doi:10.1126/science.1090110.

1517 Zeebe, R.E., Ridgwell, A., and Zachos, J.C., 2016, Anthropogenic carbon release rate unprecedented during the
1518 past 66 million years: *Nature Geoscience*, v. 9, p. 325–329, doi:10.1038/ngeo2681.

1519 Zhang, F., Dellinger, M., Hilton, R.G., Yu, J., Allen, M.B., Densmore, A.L., Sun, H., and Jin, Z., 2022,
1520 Hydrological control of river and seawater lithium isotopes: *Nature Communications*, v. 13, p. 3359,
1521 doi:10.1038/s41467-022-31076-y.

1522

Page 4: [1] Formatted Rocio Jaimes Gutierrez 07/01/2026 18:18:00

English (UK)

Page 4: [1] Formatted Rocio Jaimes Gutierrez 07/01/2026 18:18:00

English (UK)

Page 4: [1] Formatted Rocio Jaimes Gutierrez 07/01/2026 18:18:00

English (UK)

Page 4: [2] Deleted Rocio Jaimes Gutierrez 07/01/2026 17:50:00

▼
Page 4: [2] Deleted Rocio Jaimes Gutierrez 07/01/2026 17:50:00

▼
Page 4: [2] Deleted Rocio Jaimes Gutierrez 07/01/2026 17:50:00

▼
Page 4: [3] Deleted Rocio Jaimes Gutierrez 07/01/2026 17:53:00

▼
Page 4: [3] Deleted Rocio Jaimes Gutierrez 07/01/2026 17:53:00

▼
Page 4: [4] Deleted Rocio Jaimes Gutierrez 07/01/2026 21:09:00

▼
Page 4: [4] Deleted Rocio Jaimes Gutierrez 07/01/2026 21:09:00

▼
Page 4: [5] Deleted Rocio Jaimes Gutierrez 22/11/2025 17:27:00

▼
Page 4: [6] Formatted Rocio Jaimes Gutierrez 07/01/2026 18:18:00

Font: Italic

Page 4: [6] Formatted Rocio Jaimes Gutierrez 07/01/2026 18:18:00

Font: Italic

Page 4: [7] Deleted Rocio Jaimes Gutierrez 07/01/2026 21:09:00

▼
Page 4: [7] Deleted Rocio Jaimes Gutierrez 07/01/2026 21:09:00

▼
Page 4: [8] Deleted Rocio Jaimes Gutierrez 22/11/2025 17:40:00

▼
Page 4: [8] Deleted Rocio Jaimes Gutierrez 22/11/2025 17:40:00

▼
Page 4: [8] Deleted Rocio Jaimes Gutierrez 22/11/2025 17:40:00

▼
Page 4: [8] Deleted Rocio Jaimes Gutierrez 22/11/2025 17:40:00

▼
Page 4: [9] Deleted Rocio Jaimes Gutierrez 07/01/2026 16:54:00

▼
Page 4: [10] Formatted Rocio Jaimes Gutierrez 07/01/2026 18:18:00

Font: Italic

Page 4: [10] Formatted Rocio Jaimes Gutierrez 07/01/2026 18:18:00

Font: Italic

Page 4: [10] Formatted Rocio Jaimes Gutierrez 07/01/2026 18:18:00

Font: Italic

Page 4: [10] Formatted Rocio Jaimes Gutierrez 07/01/2026 18:18:00

Font: Italic

Page 4: [11] Formatted Rocio Jaimes Gutierrez 07/01/2026 18:18:00

English (UK)

Page 4: [11] Formatted Rocio Jaimes Gutierrez 07/01/2026 18:18:00

English (UK)

Page 4: [11] Formatted Rocio Jaimes Gutierrez 07/01/2026 18:18:00

English (UK)

Page 4: [12] Deleted Rocio Jaimes Gutierrez 07/01/2026 17:28:00

▼

Page 4: [13] Deleted Rocio Jaimes Gutierrez 07/01/2026 17:28:00

▼

Page 4: [13] Deleted Rocio Jaimes Gutierrez 07/01/2026 17:28:00

▼

Page 4: [14] Formatted Rocio Jaimes Gutierrez 07/01/2026 18:18:00

English (UK)

Page 4: [14] Formatted Rocio Jaimes Gutierrez 07/01/2026 18:18:00

English (UK)

Page 4: [14] Formatted Rocio Jaimes Gutierrez 07/01/2026 18:18:00

English (UK)

Page 11: [15] Formatted Rocio Jaimes Gutierrez 12/01/2026 16:52:00

Font: 10 pt

Page 11: [15] Formatted Rocio Jaimes Gutierrez 12/01/2026 16:52:00

Font: 10 pt

Page 11: [15] Formatted Rocio Jaimes Gutierrez 12/01/2026 16:52:00

Font: 10 pt

Page 11: [15] Formatted Rocio Jaimes Gutierrez 12/01/2026 16:52:00

Font: 10 pt

Page 11: [15] Formatted Rocio Jaimes Gutierrez 12/01/2026 16:52:00

Font: 10 pt

Page 11: [16] Formatted Rocio Jaimes Gutierrez 12/01/2026 16:57:00

Font: 10 pt

Page 11: [16] Formatted Rocio Jaimes Gutierrez 12/01/2026 16:57:00

Font: 10 pt

Page 11: [16] Formatted Rocio Jaimes Gutierrez 12/01/2026 16:57:00

Font: 10 pt

Page 11: [16] Formatted Rocio Jaimes Gutierrez 12/01/2026 16:57:00

Font: 10 pt

Page 11: [16] Formatted Rocio Jaimes Gutierrez 12/01/2026 16:57:00

Font: 10 pt

Page 11: [16] Formatted Rocio Jaimes Gutierrez 12/01/2026 16:57:00

Font: 10 pt

Page 11: [16] Formatted Rocio Jaimes Gutierrez 12/01/2026 16:57:00

Font: 10 pt

Page 11: [16] Formatted Rocio Jaimes Gutierrez 12/01/2026 16:57:00

Font: 10 pt

Page 11: [16] Formatted Rocio Jaimes Gutierrez 12/01/2026 16:57:00

Font: 10 pt

Page 11: [16] Formatted Rocio Jaimes Gutierrez 12/01/2026 16:57:00

Font: 10 pt

Page 11: [17] Deleted Wilson, David 08/01/2026 13:30:00

Page 13: [18] Formatted Rocio Jaimes Gutierrez 12/01/2026 14:15:00

Font: (Default) Times New Roman, Font colour: Text 1

Page 13: [18] Formatted Rocio Jaimes Gutierrez 12/01/2026 14:15:00

Font: (Default) Times New Roman, Font colour: Text 1

Page 13: [18] Formatted Rocio Jaimes Gutierrez 12/01/2026 14:15:00

Font: (Default) Times New Roman, Font colour: Text 1

Page 13: [18] Formatted Rocio Jaimes Gutierrez 12/01/2026 14:15:00

Font: (Default) Times New Roman, Font colour: Text 1

Page 13: [19] Formatted Rocio Jaimes Gutierrez 12/01/2026 14:15:00

Font: (Default) Times New Roman, Font colour: Text 1

Page 13: [19] Formatted Rocio Jaimes Gutierrez 12/01/2026 14:15:00

Font: (Default) Times New Roman, Font colour: Text 1

Page 13: [19] Formatted Rocio Jaimes Gutierrez 12/01/2026 14:15:00

Font: (Default) Times New Roman, Font colour: Text 1

Page 13: [19] Formatted Rocio Jaimes Gutierrez 12/01/2026 14:15:00

Font: (Default) Times New Roman, Font colour: Text 1

Page 13: [19] Formatted Rocio Jaimes Gutierrez 12/01/2026 14:15:00

Font: (Default) Times New Roman, Font colour: Text 1

Page 13: [19] Formatted Rocio Jaimes Gutierrez 12/01/2026 14:15:00

Font: (Default) Times New Roman, Font colour: Text 1

Page 13: [19] Formatted Rocio Jaimes Gutierrez 12/01/2026 14:15:00

Font: (Default) Times New Roman, Font colour: Text 1

Page 13: [19] Formatted Rocio Jaimes Gutierrez 12/01/2026 14:15:00

Font: (Default) Times New Roman, Font colour: Text 1

Page 13: [19] Formatted Rocio Jaimes Gutierrez 12/01/2026 14:15:00

Font: (Default) Times New Roman, Font colour: Text 1

Page 13: [19] Formatted Rocio Jaimes Gutierrez 12/01/2026 14:15:00

Font: (Default) Times New Roman, Font colour: Text 1

Page 13: [20] Deleted Rocio Jaimes Gutierrez 07/01/2026 18:13:00

x

Page 13: [20] Deleted Rocio Jaimes Gutierrez 07/01/2026 18:13:00

x

Page 13: [20] Deleted Rocio Jaimes Gutierrez 07/01/2026 18:13:00

x

Page 13: [21] Formatted Rocio Jaimes Gutierrez 07/01/2026 20:25:00

English (UK)

Page 13: [21] Formatted Rocio Jaimes Gutierrez 07/01/2026 20:25:00

English (UK)

Page 13: [22] Formatted Rocio Jaimes Gutierrez 07/01/2026 18:18:00

Font: Symbol, English (UK)

Page 13: [22] Formatted Rocio Jaimes Gutierrez 07/01/2026 18:18:00

Font: Symbol, English (UK)

Page 13: [22] Formatted Rocio Jaimes Gutierrez 07/01/2026 18:18:00

Font: Symbol, English (UK)

Page 13: [22] Formatted Rocio Jaimes Gutierrez 07/01/2026 18:18:00

Font: Symbol, English (UK)

Page 13: [22] Formatted Rocio Jaimes Gutierrez 07/01/2026 18:18:00

Font: Symbol, English (UK)

Page 13: [23] Deleted Rocio Jaimes Gutierrez 07/01/2026 21:10:00

v

Page 13: [23] Deleted Rocio Jaimes Gutierrez 07/01/2026 21:10:00

v

Page 13: [24] Deleted Rocio Jaimes Gutierrez 07/01/2026 19:19:00

v

Page 13: [24] Deleted Rocio Jaimes Gutierrez 07/01/2026 19:19:00

v

Page 13: [24] Deleted Rocio Jaimes Gutierrez 07/01/2026 19:19:00

v

Page 13: [24] Deleted Rocio Jaimes Gutierrez 07/01/2026 19:19:00

v

Page 13: [25] Formatted Rocio Jaimes Gutierrez 07/01/2026 18:18:00

No underline

Page 13: [25] Formatted Rocio Jaimes Gutierrez 07/01/2026 18:18:00

No underline

Page 13: [25] Formatted Rocio Jaimes Gutierrez 07/01/2026 18:18:00

No underline

Page 13: [25] Formatted Rocio Jaimes Gutierrez 07/01/2026 18:18:00

No underline

Page 13: [25] Formatted Rocio Jaimes Gutierrez 07/01/2026 18:18:00

No underline

Page 13: [25] Formatted Rocio Jaimes Gutierrez 07/01/2026 18:18:00

No underline

Page 13: [25] Formatted Rocio Jaimes Gutierrez 07/01/2026 18:18:00

No underline

Page 13: [25] Formatted Rocio Jaimes Gutierrez 07/01/2026 18:18:00

No underline

Page 13: [25] Formatted Rocio Jaimes Gutierrez 07/01/2026 18:18:00

No underline

Page 13: [25] Formatted Rocio Jaimes Gutierrez 07/01/2026 18:18:00

No underline

Page 14: [26] Formatted Rocio Jaimes Gutierrez 07/01/2026 18:18:00

Font: Symbol

Page 14: [26] Formatted Rocio Jaimes Gutierrez 07/01/2026 18:18:00

Font: Symbol

Page 14: [26] Formatted Rocio Jaimes Gutierrez 07/01/2026 18:18:00

Font: Symbol

Page 14: [26] Formatted Rocio Jaimes Gutierrez 07/01/2026 18:18:00

Font: Symbol

Page 14: [27] Deleted Rocio Jaimes Gutierrez 06/01/2026 22:35:00

▼

Page 14: [27] Deleted Rocio Jaimes Gutierrez 06/01/2026 22:35:00

▼

Page 14: [27] Deleted Rocio Jaimes Gutierrez 06/01/2026 22:35:00

▼

Page 14: [28] Deleted Rocio Jaimes Gutierrez 07/01/2026 11:04:00

▼

Page 14: [28] Deleted Rocio Jaimes Gutierrez 07/01/2026 11:04:00

▼

Page 14: [28] Deleted Rocio Jaimes Gutierrez 07/01/2026 11:04:00

▼

Page 14: [29] Formatted Rocio Jaimes Gutierrez 07/01/2026 18:18:00

Font: 10 pt

Page 14: [29] Formatted Rocio Jaimes Gutierrez 07/01/2026 18:18:00

Font: 10 pt

Page 14: [29] Formatted Rocio Jaimes Gutierrez 07/01/2026 18:18:00

Font: 10 pt

Page 14: [29] Formatted Rocio Jaimes Gutierrez 07/01/2026 18:18:00

Font: 10 pt

Page 14: [29] Formatted Rocio Jaimes Gutierrez 07/01/2026 18:18:00

Font: 10 pt

Page 14: [29] Formatted Rocio Jaimes Gutierrez 07/01/2026 18:18:00

Font: 10 pt

Page 14: [29] Formatted Rocio Jaimes Gutierrez 07/01/2026 18:18:00

Font: 10 pt

Page 14: [29] Formatted Rocio Jaimes Gutierrez 07/01/2026 18:18:00

Font: 10 pt

Page 14: [29] Formatted Rocio Jaimes Gutierrez 07/01/2026 18:18:00

Font: 10 pt

Page 14: [30] Formatted Rocio Jaimes Gutierrez 07/01/2026 18:18:00

Font: Symbol, English (UK)

Page 14: [30] Formatted Rocio Jaimes Gutierrez 07/01/2026 18:18:00

Font: Symbol, English (UK)

Page 14: [30] Formatted Rocio Jaimes Gutierrez 07/01/2026 18:18:00

Font: Symbol, English (UK)

Page 14: [30] Formatted Rocio Jaimes Gutierrez 07/01/2026 18:18:00

Font: Symbol, English (UK)

Page 14: [31] Deleted Rocio Jaimes Gutierrez 07/01/2026 11:08:00

▼

Page 14: [32] Deleted Rocio Jaimes Gutierrez 07/01/2026 19:21:00

▼

Page 14: [32] Deleted Rocio Jaimes Gutierrez 07/01/2026 19:21:00

▼

Page 14: [32] Deleted Rocio Jaimes Gutierrez 07/01/2026 19:21:00

▼

Page 14: [33] Formatted Rocio Jaimes Gutierrez 07/01/2026 19:24:00

Font: 10 pt

Page 14: [33] Formatted Rocio Jaimes Gutierrez 07/01/2026 19:24:00

Font: 10 pt

Page 14: [33] Formatted Rocio Jaimes Gutierrez 07/01/2026 19:24:00

Font: 10 pt

Page 14: [33] Formatted Rocio Jaimes Gutierrez 07/01/2026 19:24:00

Font: 10 pt

Page 14: [33] Formatted Rocio Jaimes Gutierrez 07/01/2026 19:24:00

Font: 10 pt

Page 14: [34] Formatted Rocio Jaimes Gutierrez 07/01/2026 19:24:00

Font: 10 pt

Page 14: [34] Formatted Rocio Jaimes Gutierrez 07/01/2026 19:24:00

Font: 10 pt

Page 14: [34] Formatted Rocio Jaimes Gutierrez 07/01/2026 19:24:00

Font: 10 pt

Page 14: [34] Formatted Rocio Jaimes Gutierrez 07/01/2026 19:24:00

Font: 10 pt

Page 14: [34] Formatted	Rocio Jaimes Gutierrez	07/01/2026 19:24:00
-------------------------	------------------------	---------------------

Font: 10 pt

Page 14: [34] Formatted	Rocio Jaimes Gutierrez	07/01/2026 19:24:00
-------------------------	------------------------	---------------------

Font: 10 pt

Page 14: [35] Deleted	Rocio Jaimes Gutierrez	07/01/2026 19:24:00
-----------------------	------------------------	---------------------

▼

Page 14: [36] Formatted	Rocio Jaimes Gutierrez	07/01/2026 20:35:00
-------------------------	------------------------	---------------------

French (Switzerland)

Page 14: [36] Formatted	Rocio Jaimes Gutierrez	07/01/2026 20:35:00
-------------------------	------------------------	---------------------

French (Switzerland)